

A Systematic Description of Shocks in Gamma Ray Bursts: I. Formulation

Houri Ziaeepour[?]

Mullard Space Science Laboratory, Holmbury St Mary, Dorking, Surrey RH5 6NT, UK

Accepted ::; Received ::; in original form Dec. 2008

ABSTRACT

Since the suggestion of relativistic shocks as the origin of gamma-ray bursts (GRBs) in early 90's, the mathematical formulation of this process has stayed at phenomenological level. One of the reasons for the slow development of theoretical works has been the simple power-law behaviour of the afterglow shows or days after the prompt gamma-ray emission. It was believed that they could be explained with these formulations. Nowadays with the launch of the Swift satellite and implementation of robotic ground follow-ups, gamma-ray bursts and their afterglow can be observed in multi-wavelength from a few tens of seconds after trigger onward. These observations have led to the discovery of features unexplainable by the simple formulation of the shocks and emission processes used up to now. Some of these features can be inherent to the nature and activities of the GRBs central engines which are not yet well understood. On the other hand devil is in details and others may be explained with a more detailed formulation of these phenomena and without adhoc addition of new processes. Such a formulation is the goal of this work. We present a consistent formulation of the kinematic and dynamics of the collision between two spherical relativistic shells, their energy dissipation, and their coalescence. It can be applied to both internal and external shocks. Notably, we propose two phenomenological models for the evolution of the emitting region during the collision. One of these models is more suitable for the prompt/internal shocks and late external shocks, and the other for the afterglow/external collisions as well as the onset of internal shocks. We calculate a number of observables such as flux, lag between energy bands, and hardness ratios. One of our aims has been a formulation enough complex to include the essential processes, but enough simple such that the data can be directly compared with the theory to extract the value and evolution of physical quantities. To accomplish this goal, we also suggest a procedure for extracting parameters of the model from data. In a following paper we numerically calculate the evolution of some simulated models and compare their features with the properties of the observed gamma-ray bursts.

Key words: gamma-rays:bursts { shockwaves.

1 INTRODUCTION

The Swift (Gehrels et al. 2004) observations of more than 200 Gamma-Ray Bursts (GRBs) and their follow-ups have been a revolution in our knowledge and understanding of these elusive phenomena. The rapid slew of the Swift X-ray and UV/optical telescopes – respectively XRT (Burrows et al. 2005) and UVOT (Roming et al. 2005) – as well as ground based robotic telescopes have permitted to observe GRBs and their afterglow in multi-wavelength from few tens of seconds after the prompt or precursor gamma-ray emission is detected by BAT (Barthelmy et al.

2005), up to days after trigger. These observations show that the emission can be essentially divided to three regimes: 1) The prompt gamma-ray emission which can be very short, few tenth of milliseconds, or long, up to few hundred of seconds; 2) A tail emission in X-ray which is observed for more than 90% of bursts. For some bursts this tail is also detected as a soft faint continuum in gamma-ray. In about 40% of bursts this early emission has been detected in optical and infrared too. In this regime for many bursts there have been observed mainly in X-ray. Sometimes the counterpart of these have been also observed in gamma-ray and/or optical/IR. In many bursts the early steep slope of the X-ray emission at the beginning of this regime becomes much shallower and somehow harder at the end; 3) The late emission

[?] Email: hz@sslulac.ac.uk

can be considered as the epoch after the break of shallow regime in which the emission is usually a continuum and no or little varying activity is observed (but there are exceptions such as GRB 070110 (Krimm et al. 2007) and GRB 081028 (Guidorzi et al. 2008) which had bright late phases). The duration and relative fluxes of these regimes can vary significantly between GRBs.

In one hand, it seems that the idea of synchrotron emission from accelerated particles in a relativistic shock as the origin of the prompt emission (Rees & Meszaros 1994, 1998) is essentially correct. On the other hand, the early observations of what is usually called the afterglow – the emission in lower energy bands usually observed from ~ 100 sec after trigger onward – have been the source of surprises and raised a number of questions about many issues: the activity (Fan & Wei 2005) and the nature of the engine (Petrovic et al. 2005; Fryer et al. 2006; Gal-Yam et al. 2008), the concept of prompt/internal-afterglow/external shocks (Ramirez-Ruiz & Granot 2007), the efficiency of energy transfer from the outflow – the reball – to synchrotron radiation (Zhang et al. 2006), the collimation and jet break (Covino et al. 2006), the behaviour of X-ray and optical light curves (Panaitescu & Vestrand 2008), etc. Many of predictions such as the existence of a significant high latitude emission with a strict relation between the light curve time evolution slope and the spectrum index, and an achromatic jet break have not been observed. Moreover, the origin of unexpected behaviours such as a very steep decline in low energy bands after the prompt (Zhang et al. 2007b) and a very shallow regime which lasts for thousands of seconds are not well understood. Other unexpected observations are the existence of the chromatic multiple breaks in the X-ray light curves, phases in X-ray and optical bands hundred of seconds after the prompt even in some short bursts (ex: GRB 060313 (Pagnani et al. 2006; Roming et al. 2006), GRB 070724A (Ziaeeipour et al. 2007a), a tail emission in short bursts (ex: GRB 070714B (Racusin et al. 2007; Bradley 2008), GRB 080426 (Ziaeeipour et al. 2008b), GRB 080503 (Mao et al. 2008)), and very short, hard, and high amplitude spikes in long bursts that could lead to the classification of the burst as short if the instrument was not enough sensitive to detect the rest of the prompt emission (ex: GRB 060614 (Mangano et al. 2007; Gehrels et al. 2006), GRB 061006 (Schady et al. 2006a)). This makes the classification of bursts as short and long much more ambiguous (Zhang et al. 2007a).

One conclusion that has been made from these observations is that the central engine can be active for up to thousands of seconds after the prompt emission (Fan & Wei 2005). But the nature of the reball and its source of energy is not yet well understood, and we can not yet verify this interpretation or relate it to any specific process in the engine. It seems however that whatever the origin of the reball, it must be baryon dominated otherwise it could not make long term effects correlated to the prompt emission. In this case, the internal and external shock models as the origin of the prompt and afterglow are good candidates. Nonetheless, the lack of a simple explanation for the observed complexities has encouraged authors to consider other possibilities, for instance associating both the prompt gamma-ray and the afterglows to external shocks and fast variations to abrupt density varia-

tion of the surrounding material (Ramirez-Ruiz & Granot 2007). However, it has been shown that in such models it is not possible to explain the fast variations of the prompt even in presence of a bubbly environment or pulse-like density change (Ramirez-Ruiz & Granot 2007; Nakar & Granot 2007).

Here we suggest that at least some of the features of early afterglows can be related to a complex shock physics and/or features in the reball/jet. In fact, simulations of the acceleration of electrons and positrons by the first and second Fermi processes show that the evolution of electric and magnetic fields as well as the energy distribution of accelerated particles are quite complex (Bednarz & Ostrowski 1996; Rieger et al. 2007; Dieckmann et al. 2006). Plasma instabilities lead to the formation of coherent electric and magnetic fields and acceleration of particles (Yang et al. 1994; Wiersma & Achterberg; Silva et al. 2002; Reville et al. 2006). Their time evolution in relativistic shocks can significantly affect the behaviour of the prompt and the afterglow of GRBs. If the number density of particles in the ejecta is significant and the shock is collisional, the state of matter in the jet can be also an important factor in determining the behaviour of the fields, and thereby the synchrotron emission by accelerated electrons and positrons. Many aspects of these processes are not well understood, however realistic interpretations of observations should consider these complexities at least phenomenologically. For instance, the simple distributions such as a power-law distribution for Lorentz factor of electrons, or a constant magnetic field for the whole duration of prompt and afterglow can be quite unrealistic. Ideally, these quantities should come from the simulation of Fermi processes and plasma instabilities such as Weibel instability (Yang et al. 1994; Wiersma & Achterberg) that produces the coherent transverse magnetic field. However, these phenomena are complex and their simulations are very time and CPU consuming. For these reasons they can not yet explore the parameter space of the phenomena and are mostly useful for demonstrating the concepts and how they work. Therefore we are obliged to use simple analytical approximations for quantities related to the physics of relativistic shocks. In this situation a compromise between complex non-analytical expressions and too simplistic and too simplified but unrealistic analytical behaviour of the physical quantities can be the consideration of intervals in which a simple analytical function can be a good approximation. Then, by adding together these intervals – regimes – one can reconstruct the entire evolution of a burst and its afterglow.

Even with a simplified presentation of the physical processes one would not be able to explain GRB data without a model including both microphysics and dynamics of the reball. The majority of works on the modelling of shocks and synchrotron emissions either deal with the emission (Sari & Piran 1995; Sari et al. 1996, 1998; Nakar & Piran 2004; Zhang & Kobayashi 2005) or with the kinematics of the shock (Blandford & McKee 1977; Piran et al. 1993; Fenimore et al. 1996), or both but in a phenomenological way (Rhoads 1999). Few works (Daigne & Mochevitch 1998, 2003) have tried to include both these aspects in a consistent model, but either they have not been very successful – their predictions specially for quantities such as lags in different bands were far

from observed values and additional parametrization was necessary – or the formulation is too abstract to be compared directly with data (Vettri 2003; Blasi & Vettri 2005).

With these issues in mind, in Sec. 2 we present a simplified shock model that includes both the kinematics of the ejecta and the dynamics of the synchrotron emission. The microphysics is included by the means of a simple parametrization. We calculate a number of observables such as flux, hardness ratios, and lags between different energy bands. In this paper and paper II in which we simulate part of prompt and afterglow regimes of GRBs in some time intervals, we show that this model can explain many aspects of bursts as long as we divide the data to separate regimes. The reason is that the simple parametrization of microphysics in this model can be valid at most in a limited time interval. Each regime should be separately compared to analytical and numerical results for extracting the parameters. The results will show how parameters that are considered as constant in this model evolve during the lifetime of the burst. This is the best we can do until a better understanding of relativistic shock models and Fermi processes become available. If the model and the estimation of its parameters for each regime is sufficiently correct, adding them together should give us an overall consistent picture of characteristics of the burst, its afterglow, and its surrounding material. A priori this knowledge should help to better understand the engine activities and eventually its nature and classification.

The model presented here depends on a large number of parameters and we need an extraction procedure permitting to extract as much as possible information about the physical properties of the shock from the available data. In Sec. 3 we explain how in the framework of this model one can extract various quantities from data. Evidently the success of the modelling strongly depends on availability and quality of simultaneous multi-wavelength observations.

The Swift observations show that during the first few hundred seconds after the trigger there is usually a very close relation between the prompt gamma-ray emission and the emission in lower energy bands (Mészáros 2007; Kumar et al. 2006), therefore, most probably they have a common origin, presumably internal shocks. However, historically and even in the present literature (and sometimes believes) any emission after the prompt gamma-ray is called the afterglow – meaning due to a shock with ISM or surrounding material, presumably external shocks. Therefore, for clarity of context here we define the afterglow as the emission in any energy band and at any time after the main prompt peaks regardless of its origin. If by afterglow we mean the external shocks, this is mentioned explicitly in the text.

We finish this paper with some outlines and two appendices containing the details of calculation of the dynamics and flux for power-law distribution of electrons Lorentz factor.

2 SHOCK MODEL

In this section we first give a sketch description of a relativistic collision between two shells of material and processes which produce gamma-ray and other radiations. Then, we discuss a simplified mathematical formulation of the evolution of the shock and synchrotron emission. By restricting

the model to a thin layer and to the early times after beginning of the collision, we can analytically calculate various observables.

2.1 Qualitative description of a relativistic shock and its simplified model

We begin this section by a pictorial description of present beliefs about the origin of GRBs and their afterglow. A central source – supernova, collapsar, collision of two compact objects, etc. – ejects highly relativistic cold baryon dominated material as a spherical, jet or torus-like shells call the reball. Collision between faster later ejected shells with slower earlier ejected ones produces what is called the prompt emission (Rees & Mészáros 1994).

A priori, there is no reason why faster shells should be ejected later. One way of explaining this paradigm is the deceleration of the front shells (Fenimore & Ramirez-Ruiz 1999) by surrounding material which are observed around massive objects such as Wolf-Rayet (WR) stars (Eldridge et al. 2006). It is possible that this initial deceleration is the source of a weak emission which has been seen before the main spike in many bursts. A relatively weak and soft precursor spike has been also observed in some bursts and can be related to this deceleration (Umeda et al. 2005). Although other origins such as jet-star interaction (Lazzati et al. 2006, 2007) and fallback to the collapsar (Wang & Mészáros 2007) are also suggested to explain precursors, deceleration of the initial shell seems to be a more natural explanation and does not need any fine tuning of the progenitor models and their parameters. In contrast, jet-star interaction scenario can not explain large time lag – few 100 of seconds between precursor and the main spike in some bursts e.g. GRB 050820A (Page et al. 2005; Cenko et al. 2006), GRB 060124 (Holland et al. 2006; Romano et al. 2008), and GRB 070721B (Ziaeeipour et al. 2007b). In the fallback scenario a weak jet is produced during the formation of a transient neutron star which later collapses to a black hole. The main jet in this scenario is produced by the accretion of the material from a disk to the black hole. In this case, the lag depends on the lifetime of the proto-neutron star and the rate of the accretion from the surrounding disk. Although these parameters can be tuned to explain the lag, a priori much longer lags should be also possible but never observed. In the deceleration scenario the maximum possible lag is the duration of the central engine main activity – few hundred of seconds according to the observations of the main fares in X-ray, and is consistent with all the observations. The UV emission from the precursor should ionize the unshocked material in front of the first shell and therefore there would be little additional absorption of soft X-ray later (Watson et al. 2007). In fact in GRB 060124 (Holland et al. 2006; Romano et al. 2008) which had long lag between the precursor and the main peak, a slight increase in N_H column density at late time with respect to the initial density has been detected. In Paper II we argue that another possible origin of the precursor is the temporary dynamical reduction of the emission in the early stage of the shock that make the burst unobservable for a short time. Then, with the progress of coalescence of the shells the emission resumes and is observed as the main peak.

When two high density shells collide, in the most gen-

eral case they partially coalesce. Then, the most energetic particles get ahead of the rest in the downstream, and at the end of the collision the configuration includes again two shells. The back shell consists of slower particles that have lost their kinetic energy (shocked particles). The front shell is the remnant of faster unscattered particles in the shells. In practice we expect that the kinetic energy difference be continuous and slower particles become an expanding tail behind a faster and most probably denser head. In few bursts such as GRB 060607A (Ziaeeepour et al. 2006b, 2008a) and GRB 070107 (Stamatikos et al. 2007) it seems that we are seeing the separation between these components in the X-ray afterglow. Fig.1 shows a sketch of the shock processes.

In the simplest case the shock between two shells is radiative. This means that for an observer in the rest frame of the fast shell the kinetic energy of the falling particles from the other shell is immediately radiated and particles come to rest and join the shell. For a far observer at rest with respect to the engine the difference between the kinetic energy of the two shells is partially radiated and partially transferred to the particles of the slower shell. The fast shell is decelerated until the totality of the slow shell is swept.

Not all the particles in the fast shell are decelerated with the same rate. Therefore after the coalescence of the shells there is a gradient of Lorentz factor from the shell front head with highest to the back tail with lowest. In the macroscopic treatment of the shock processes it is usually assumed that during the collision two distinguishable shocked layers and corresponding discontinuities are formed in each side of the boundary between the shells. They are called forward and reverse shocks according to their evolution direction with respect to the initial discontinuity (Sari et al. 1996; Nakar & Piran 2004; Zhang & Kobayashi 2005). According to these models and depending on the density difference of the shells and their relative Lorentz factor, the induced electric and magnetic fields and thereby the distribution of accelerated electrons and their synchrotron emission in these shocked regions can be very different. Notably the reverse shock is expected to emit mostly in optical wavelength with a relatively large lag with respect to the prompt gamma-ray as the emission must traverse the width of both shocked layers. Therefore it should appear as an optical flash asynchronous from gamma-ray peaks (Kobayashi 2000).

On the other hand, if shells have similar densities and a small relative Lorentz factor, the scattering of particles in the two sides of the boundary quickly homogenizes the shocked regions, and therefore one can consider a single shocked zone with a relatively slow gradient in density and fields. If one of the shells has a density much larger than the other, the width of its shocked layer would be very small with respect to the shocked region in the other shell and again the assumption of a single shocked layer is a good approximation for internal shocks. This schematic view corresponds well to what is observed in the simulations of Fermi acceleration in the ultra-relativistic shocks (see Fig.1 of Spitkovsky (2008) and Keshet et al. (2008)).

For a far observer who only detects photons from the synchrotron emission of the shocked material it is very difficult to distinguish between photons coming from distinct regions unless they are well separated in time and in energy band. The lack of a clear evidence for a reverse shock emission in the Swift bursts, specially during the prompt

emission, means that the reverse shock in the prompt GRB emission is weak and the assumption of just one shocked region is a good approximation. Most of the synchrotron emission is expected to be emitted by charged particles in the shocked region. But as electric and magnetic fields, and accelerated particles are not really confined in this region and penetrate to a larger area, the region that emit radiation can be much extended than shocked region. We call this emitting zone the active region.

Evidently, in a real situation multiple shells are ejected in a short time interval. In this case both pair collisions between late shells and collision-coalescence of the late shells with the main ejecta - prompt shell - is possible. These events happen at different points of space-time, but their synchrotron emission can arrive to the observer separately, partially overlapping, or simultaneously. Therefore it is not always possible to distinguish separate collisions and their characteristics. To this complexity one must also add the variation of quantities such as density and Lorentz factor in a single shell. They increase the variability of observed emissions. On the other hand, overlapping emissions make the comparison of data with the models based on a simple parametrization of the physical properties of a shell ambiguous. Despite these complexities one should be able to consider peaks as separate collisions and find an effective set of parameters to model each one separately.

2.2 Shock evolution

A shock is defined mathematically as a discontinuity in the density distribution of a flow. It should satisfy at each point of the space-time the total energy-momentum and current/particle flux conservation equation (Anile 1989):

$$T_{;\mu} = 0 \quad (1)$$

$$\sum_i (j_i u_i)_{;\mu} = 0 \quad (2)$$

where T is the total energy-momentum tensor; ρ is density and u velocity vector; the index i indicates species of particles/ fluids with a conserved number. They also include the interactions between these particles/ fluids. When there is no interaction, these equations must be satisfied separately for each species. In particular, at the shock front where these quantities are discontinuous the conservation equations take the form of jump conditions across the discontinuity surface:

$$[T] = 0 \quad (3)$$

$$\sum_i [j_i u_i] = 0 \quad (4)$$

The symbol $[]$ means the difference of the quantities between square brackets on the two sides of the shock front. Solutions of these equations determine the evolution of the shock front. As for the state of the shocked material behind the discontinuity, when there is no energy dissipation jump conditions can be used to obtain a self-similar solution (Blandford & McKee 1977). In presence of energy injection or dissipation however the self-similarity solutions are only approximations and in general an exact self-similar solution does not exist. Moreover, energy dissipation by synchrotron emission changes the form of the conservation

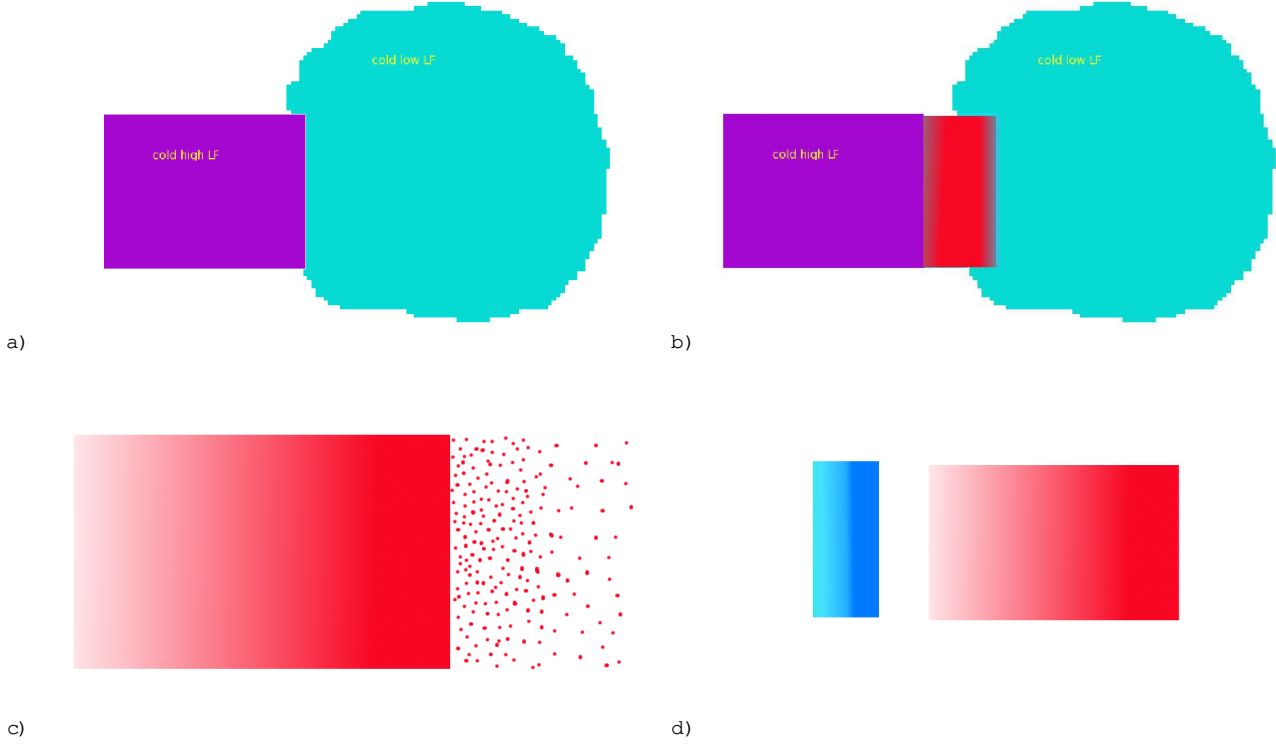


Figure 1. Sketch of a relativistic shock: a) Beginning of the shock: A high Lorentz factor cold shell (violet) moving from left to right collides with a slower shell or ISM (blue). b) During the passage of the shells through each other, at the shock front an active region is formed where large electric and orthogonal magnetic fields are induced by plasma instabilities and charged particles are accelerated. They lose part of their kinetic energy as a synchrotron emission. The concept of active (emitting) region is not new and is commonly used in the context of the formation of cosmic rays in relativistic and non-relativistic shocks by Fermi processes (Virtanen & Vainio 2005b,a). A fraction of these highly accelerated particles escape to the downstream. By contrast, particles that have lost their energy move toward upstream. This process extends the active region but reduces the gradient of quantities such as density, thus gradually weakens the shock. c) and d) show two possible outcome of the collision: total coalescence of the shells (radiative collision) c) and when after the passage of the fast shell a left-over slow shell is formed behind. In these figures colour gradient presents the velocity and density distributions: darker colours correspond to higher velocity/density.

equations, i.e. it can not be treated as an inhomogeneous term in the differential equations describing the dynamics. Thus, it is not possible to extend the solutions of the non-dissipative case to this case even as an approximation. We will discuss this issue in details later in this section. Therefore in a dissipative shock the jump conditions are applied only at the initial time when a shell meets another shell or the ISM, and they should be considered as boundary conditions when conservation equations (1) and (2) are solved.

Intuitively we expect that with time the discontinuous distributions of quantities in the shock front i.e. the initial jump conditions change to continuous distributions which at far downstream distances should asymptotically approach to the slow shell values, and at far distances in the upstream direction to the characteristics of the fast shell – see Fig.1 for a schematic illustration. In this transient region instabilities form electric and transversal magnetic fields. They accelerate electrons which subsequently lose their energy by synchrotron and inverse Compton emission. A far observer receives the signature of the shock mainly through the detection of these radiations as γ -ray burst or X-ray are. Therefore finding the evolution of physics of this region is the main purpose for solving conservation equations.

A full solution of equations (1) and (2) with the initial conditions (3) and (4) a priori include all the necessary information about the physical processes and their evolution. However, the complexity of the problem can not permit to solve them analytically. On the other hand, numerical simulations are both complex and time consuming, and it would be very difficult to cover the full parameter space and obtain results that can be compared with the observations. At present, simulations are only able to demonstrate the validity of ideas about processes involved and the role of the instabilities in the formation of coherent fields (Spitkovsky 2008; Keshet et al. 2008).

Here we consider an intermediate strategy. We assume a spherical¹ thin and optically transparent active region. Its average distance from the central source is $r(t)$ and its thickness $\Delta r(t)$. We neglect the variation of quantities inside the active region and consider the average value through the region. This means that the evolution depends only

¹ Most of the formulation presented here is also applicable to a beamed ejecta/jet if the transverse dispersion of matter in the jet is negligible with respect to the boost in the radial direction. We consider the effect of beaming in Sec.2.6

on $r(t)$ the mean distance of the active region from central engine. As for the energy dissipation, we assume a radiative shock i.e. for an observer at rest with respect to the active region the incoming particles lose their energy through synchrotron radiation and join this region. Despite possibility of large contribution from Compton cooling of electrons in the GRBs prompt (Stern & Poutanen 2004; Piran et al. 2008), X-ray fares (Kobayashi et al. 2007), and afterglow (Wang et al. 2001), there is no strong evidence of this process in the Swift data. Cases such as the early are of GRB 050406 (Romano et al. 2006) that was once attributed to Compton cooling of a reverse shock is now understood to be related to the late activity of the central engine like all other observed fares and have the same origin as the gamma-ray. It is also suggested that the anomalous behaviour of GRB 060218/SN 2006aj (Soderberg et al. 2006) is due to inverse Compton cooling (Dai et al. 2006), but this is an exception. Therefore here we only consider synchrotron radiation in a relativistic shock as the source of emission.

From now on we consider the active region as an isolated shell of baryonic material. The effect of ISM/slow shell appears as an incoming flux, and the effect of diffusion of shocked material into the upstream is included in the evolution of the thickness of the active region and other physical parameters such as density variation with time. The initial value of the density and Lorentz factor correspond to the values in the fast shell i.e. the shock front at the time of encounter between the two shells (internal shock) or fast shell and the ISM (external shock). We also assume that thermal energy and pressure are negligible with respect to the relativistic boost. This assumption of cold matter is specially justified for the prompt emission because the temperature of ejected material from the progenitor is expected to be at most a few hundred MeV, where the kinetic energy of relativistic baryons must be of order of few GeV or larger. This approximation is not probably suitable for late interaction of the shells when they have lost most of their kinetic energy and probably turbulence and scattering have transferred part of this energy to thermal.

With these approximations we write the energy-momentum conservation equations for the active region in the rest frame of the slow shell. The reason for choosing this frame is that the same formulation can be applied to external shocks where the slow shell is the ISM or surrounding material around the engine. The latter is considered to be at rest with respect to the observer (after correction for the expansion of the Universe)². Note that for the consistency and conservation of energy and momentum we have to integrate equations (1) and (2) along the active region. As we only consider the average value of quantities, the integration

is trivial³:

$$\frac{d(r^0 n^0 r^0)}{dr} = \left(r^0 \frac{d(n^0 r^0)}{dr^0} + 2r^0 (n^0 r^0) \right) + r^0 (n^0 r^0) \frac{d}{dr^0} = n_0^0(r) r^0 \frac{dE_{sy}^0}{4 m c^2 dr^0} \quad (5)$$

$$\frac{d(r^0 n^0 r^0)}{dr^0} = \left(r^0 \frac{d(n^0 r^0)}{dr^0} + 2r^0 (n^0 r^0) \right) + r^0 (n^0 r^0) \frac{d(\gamma^0)}{dr^0} = \frac{dE_{sy}^0}{4 m c^2 dr^0} \quad (6)$$

where r^0 is the distance from the central engine, n^0 is the baryon number density of the fast shell measured in the slow shell frame, n_0^0 is the baryon number density of the slow shell in its rest frame and in general it can depend on r^0 . Here we assume that $n_0^0(r^0) = N_0(r^0=r_0^0)$. For ISM $\gamma^0 = 0$, i.e. no radial dependence. For a wind surrounding the central engine $\gamma^0 = 2$ is usually assumed (Chevalier & Li 2000). For a thin shell or jet expanding adiabatically also $\gamma^0 = 2$ if we neglect the transverse expansion in the case of a jet (collimated ejecta). But for the collision between two thin shells if the duration of the collision is much smaller than r_0^0/c we can neglect the density change due to expansion during the collision, and assume $\gamma^0 = 0$. r^0 is the thickness of the shocked synchrotron emitting region, γ^0 is the Lorentz factor of the fast shell with respect to the slow shell, $\gamma^0 = \sqrt{1 - v^2/c^2}$, $m = m_p + m_e$, E_{sy}^0 is the total emitted energy, and c is the speed of light. The evolution of the radius with time is:

$$r^0(t^0) - r^0(t_0^0) = c \int_{t_0^0}^{t^0} \gamma^0(t^0) dt^0 \quad (7)$$

where the initial time t_0^0 is considered to be the beginning of the collision.

A priori we should also consider a conservation equation for the baryon and lepton numbers. However, with approximations explained above the thickness of the active region is a parameter which is added by hand. The simplest assumption is that the active region is formed only from particles that fall from the slow shell to the shock front and they stay there. In this case the baryon number conservation is simply:

$$\frac{d(n^0 r^0)}{dr^0} = n_0^0 \quad (8)$$

On the other hand the assumption of particles staying forever in the active region seems quite unphysical because scattering, acceleration, and dissipation move shocked particles to both upstream and downstream and gradually many of particles are in a region where instabilities are too weak to make the electric and magnetic fields necessary for the acceleration and synchrotron emission. Therefore in this approximation the active region can not be considered as a completely isolated system with full conservation laws applied to it. The consequence of this is that we can not determine r from first principles. This point can be also interpreted as the manifestation of the fact that there is not an abrupt termination of the active zone, and therefore there is no conservation for the artificial boundary we have added by hand.

² Throughout this work frame-dependent quantities with a prime are measured with respect to the rest frame of the slow shell and without prime with respect to a far observer at the redshift of the central engine. Parameters used for parametrization do not have a prime even when parametrization is in the slow shell frame.

³ Note also that a priori we should consider an angular term representing the collimation of the radial element. But for an infinitesimal element the angular dependence is negligible and we do not add it to this formulation.

In fact it is equally valid if we consider a conserved number of particles and the corresponding conservation equation but give up energy or momentum conservation. In this definition the active region follows active particles (in an Hamiltonian formulation sense). However, the only measurable quantity for a far observer is the energy dissipated as radiation. Therefore, it is more useful to define the active region based on the energy-momentum conservation and leave the number of these particles as a free parameter. Note also that in the left hand side of (5) and (6), as well as in the synchrotron term under some conditions (see below), $n^0 r^0$ always appears as $n^0 r^0$ i.e. the column density. It is more relevant for the observations and does not depend on the way we define the active region.

We can formally integrate equation (5) by replacing the synchrotron term in the left hand side of (6), and determine the column density of the active region⁴:

$$n^0 r^0 = \frac{N_0 r_0^3 \left(\left(\frac{r^0}{r_0} \right)^3 - 1 \right) + (3 - \gamma) n^0(r_0) r^0 (r_0)^0 (1 - \frac{r^0}{r_0})}{(3 - \gamma) r^0 (1 - \frac{r^0}{r_0})} \quad (9)$$

where $\frac{r^0}{r_0}$ and $n^0(r_0)$ is the corresponding r^0 . This solution depends on the evolution of r^0 which can be obtained by solving (6), but we first remind the dependence of the synchrotron term on the microphysics of the shock. The power of synchrotron radiation emitted by the active shell is:

$$P^0 = \frac{dE_{sy}^0}{dt^0} = c \frac{dE_{sy}^0}{dr^0} = \frac{16}{3} r^0 r_0^0 \tau c \frac{B^0}{8} \int n_e^0(\epsilon) \epsilon^2 d\epsilon \quad (10)$$

where n_e^0 is the number density of accelerated charged leptons – electrons and possibly positrons – with a Lorentz factor ϵ in the active region (shock) frame, B^0 is the magnetic field – $B^0 = 8$ is the magnetic energy density in the active region frame, and τ is Thompson cross-section. We define the normalization of electron distribution as the following:

$$\int_m^1 n_e^0(\epsilon) d\epsilon = n_a^0 \quad (11)$$

$$\int_m^1 \epsilon n_e^0(\epsilon) d\epsilon = \frac{\omega_m p n_0^0}{m_e} \quad (12)$$

where n_a^0 is the number density of accelerated charged leptons and ϵ is the fraction of the kinetic energy of the falling baryons transferred to the accelerated leptons in the active region frame.

In GRB/relativistic shock literature it is usually assumed that $n_a^0 = n_0^0$, i.e. only falling leptons are accelerated. However, the validity of this assumption is not certain because once the electric and magnetic fields are produced by the instabilities, all the charged leptons are accelerated. If the initial number density of charged leptons in the rest frame of the shells is similar to the slow shell, then as the flux of falling leptons is enhanced by a factor of γ^0 , the density of local leptons can be neglected. However, in prompt

collision one expects that the relative Lorentz factor of the shells be $O(1)$. In this case the local density of leptons is not negligible and $n_a^0 = (n_{te}^0 + n_{tp}^0)$, with n_{te}^0 and n_{tp}^0 respectively the total number density of electrons and positrons. For a neutral matter with negligible positrons content $n_a^0 = n_{te}^0$.

Motivated by the power-law distribution of accelerated charged particles in other astronomical shocks, e.g. supernovae and cosmic rays, it is usually assumed that the distribution of accelerated electrons responsible for the GRB prompt and afterglow emission is a power-law:

$$n_e^0(\epsilon) = N_e \left(\frac{\epsilon}{m} \right)^{-(p+1)} \quad \text{for } \epsilon > m \quad (13)$$

$$N_e = \frac{n_a^0 p}{m} = \frac{p^2 m_e n_a^0}{(p-1) \epsilon^{\omega_m p} n_0^0} \quad (14)$$

$$m = \frac{(p-1) \epsilon^{\omega_m p} n_0^0}{p m_e n_a^0} \quad (15)$$

Recent simulations of particle acceleration by Fermi process in the relativistic shocks show (Spitkovsky 2008) that $n_e^0(\epsilon)$ is best fitted by a 2D Maxwellian distribution plus a power-law with an exponential cutoff:

$$n_e^0(\epsilon) = C_1 e^{-\epsilon} \exp(-\epsilon - 1) + C_2 e^{-m \ln[1; \exp(-\epsilon - i) = \text{cut}]]} \quad (16)$$

where $C_2 = 0$ for ϵ less than a minimum value m_{in} . The typical values of parameters obtained from the fit to simulations for an initial Lorentz factor of $\gamma_0 = 15$ are: $m_{in} = 40$, $i = 6$, $i = 300$, $\text{cut} = 100$, and $\gamma = 2.5$ (Spitkovsky 2008). Implementation of this distribution makes the model presented here significantly more complex. In the range of energies relevant to the prompt and early afterglow emission of GRBs, the first term in (16) is negligible and for $\epsilon > i$ the distribution has the form of a power-law with exponential cutoff. Conservation conditions similar to (14) and (15) for this distribution lead to the following relations:

$$n_e^0(\epsilon) = N_e \left(\frac{\epsilon}{m} \right)^{-(p+1)} m \ln[1; \exp(-\epsilon - i) = \text{cut}]] \quad (17)$$

$$n_a^0 = \frac{N_e m}{p} \left[1 - \left(\frac{i}{m} \right)^p + p \left(\frac{\text{cut}}{m} \right)^p \exp\left(-\frac{i}{\text{cut}}\right) \left(p; \frac{i}{\text{cut}} \right) \right] \quad (18)$$

$$\frac{\omega_m p n_0^0}{m_e} = \frac{N_e m^2}{(p-1)} \left[1 - \left(\frac{i}{m} \right)^{p-1} + (p-1) \left(\frac{\text{cut}}{m} \right)^{p-1} \exp\left(-\frac{i}{\text{cut}}\right) \left((p-1); \frac{i}{\text{cut}} \right) \right] \quad (19)$$

where $(\gamma; x)$ is the incomplete Gamma function. As the number of parameters in this distribution is larger than the number of conservation conditions, in contrast to the power-law distribution, it is not possible to find an expression for N_e and m with respect to the total density and the fraction of electric and magnetic energies transferred to leptons. A more simplified version of this model is a power-law with an

⁴ We remind that column density and total power are scalars and therefore their value is frame independent

exponential cut-off :

$$n_e^0(r) = N_e \left(\frac{r}{r_0} \right)^{-(p+1)} \exp\left(-\frac{r}{r_{\text{cut}}}\right) \quad \text{for } r > r_m; \quad r_{\text{cut}} > r_m \quad (20)$$

Note that due to the exponential cut-off the restriction to $p > 2$ does not apply and the index of the power-law term can be negative. Using conservation conditions (11) and (12) we can find relations between parameters of this distribution:

$$r_{\text{cut}} = \frac{q_m n_p n_a^0}{p j_e n_a^0} \quad (21)$$

$$m N_e = n_a^0 \left(\frac{r_{\text{cut}}}{r_m} \right)^p j_e \left(p; \frac{r_{\text{cut}}}{r_m} \right) j^{-1} \quad (22)$$

As we have only two constraints, it is not possible to find expressions for 3 constants N_e , r_{cut} , and r_m , and one of them will stay as free parameter. In Sec.2.4 we show that this type of electron distribution is necessary to explain the hard spectrum of the short hard and some of the long bursts.

In the introduction we mentioned that the induced transverse magnetic field is produced by Weibel instability in the active region. The magnetic energy density is parametrized by assuming that it is proportional to the energy density of in-falling particles to the shock front/active region:

$$\frac{B^2}{8} = \beta_c^2 \frac{1}{2} m_p n_0^0 \quad (23)$$

It is expected that both n_e and B evolve with time/radius. If the central engine is magnetized the external magnetic energy can be very important and an external field should be added to the right hand side of (23). Here for simplicity we neglect such cases.

Considering the simplest case of a power-law distribution for electrons and also assuming that only in-falling electrons are accelerated i.e. $n_a^0 = n_0^0 - n_0^0$ (n_0^0 is the minimum of n_a^0 for a radiative shock), the synchrotron term in (5) and (6) becomes:

$$\frac{dE_{\text{sy}}}{4 \pi m c^2 dr^0} = \frac{4 \pi T_p n_0^0 \frac{1}{2} \beta_c^2 \frac{1}{2} m_p n_0^0}{3 m_e^2 n_0^0} \frac{r^0}{r_0^0}; \quad \frac{(p-1)^2}{p(p-2)} \quad (24)$$

For the reasons explained in the introduction and in Sec.2.1 we believe that in a realistic model of relativistic shocks one should consider the time evolution of electric and magnetic fields. Here we assume a simple power-law evolution with a constant index:

$$n_e = n_e(r_0^0) \left(\frac{r^0}{r_0^0} \right)^{-\alpha}; \quad B = B(r_0^0) \left(\frac{r^0}{r_0^0} \right)^{-\beta} \quad (25)$$

Using (24), the expression for the column density (9), and the momentum conservation equation (6), we obtain the following equation for the evolution of the relative Lorentz factor:

$$\frac{d}{dr^0} \left[\frac{N_0 r_0^0 \left(\left(\frac{r^0}{r_0^0} \right)^3 (1 + (3-\beta) \frac{1}{2} \beta_c^2 n(r_0^0) r^0 (r_0^0)^{-\alpha} (1 - \frac{1}{2} \beta_c^2) \right)}{(3-\beta)(1-\alpha)} \right] = \frac{4 \pi m_p^2 T_p N_0^2 \frac{1}{2} \beta_c^2 (r_0^0)^{-\beta} (r_0^0)^{-\alpha} r^0 \left(\frac{r^0}{r_0^0} \right)}{3 m_e^2 n_0^0} \quad (26)$$

The parameter $2\alpha + \beta + 2$ is the evolution index of

the density and fields. Although this differential equation is of order one, it is highly non-linear. To solve it we proceed a perturbative method based on iteration. Moreover, it depends explicitly on r^0 and as we discussed in Sec.2.2 to be able to find an explicit solution for $r^0(r^0)$, we have to model its evolution. We consider two models:

2.2.1 Dynamically driven active region

Assuming that the shock strength and consequently r depends mainly on the density difference, and that the densities of the shells in their rest frame are roughly the same, we expect smaller r^0 for larger β_0 . On the other hand when the relative Lorentz factor is small and the shock is soft, r^0 should be proportional to β_0 and $r^0 \rightarrow 0$ when $\beta_0 \rightarrow 0$. The simplest parametrization of r^0 with this properties is:

$$r^0 = r_0^0 \left(\frac{\beta_0}{\beta_0^0} \right) \left(r^0 - r_0^0 \right) \quad (27)$$

where r_0^0 is a thickness scale. A θ -function is added to (27) to explicitly indicate that the expression is valid only for $r^0 > r_0^0$. Note that in this model the initial thickness is not null and therefore it is assumed that it was formed in a negligible time or the value of r_0^0 is the final value from a previous regime that makes the initial active region before (27) can be applied. This model should be suitable for the prompt/internal shocks in which two high density narrow shells pass through each other and one expects that roughly instantly a narrow and dense active region forms around the shock discontinuity (See also next section for other cases). As $\beta_0 = 0 < 1$ is expected to be a decreasing function of r^0 , for $\beta_0 > 0$ the width of the active region decays and for $\beta_0 < 0$ it grows. But it is not always the case, see simulations in Paper II.

2.2.2 Quasi-steady active region

At the beginning of a strong shock, presumably an internal shock or when the slow shell is extended, roughly homogeneous, and has a low density, we expect that after a transient time in which the active region grows, its thickness arrives to a stable state determined by the relative Lorentz factor, density, synchrotron emission, and expansion of the shells. This stability should persist until the loss of kinetic energy due to radiation and mass accumulation becomes important, or the fast shell passes through the slower one (this does not happen for a radiative shock). In this case we parametrize the time evolution of r^0 as:

$$r^0 = r_1 \left[1 - \left(\frac{r^0}{r_0^0} \right) \right] \left(r - r_0^0 \right) \quad (28)$$

where r_1 is the final width when the equilibrium is achieved. For the decay of the active region at the end of this regime one can use the dynamical model. Another possibility is to consider:

$$r^0 = r_1 \left(\frac{r^0}{r_0^0} \right) \left(r - r_0^0 \right) \quad (29)$$

In Appendix A we argue that with small modifications the calculation of dynamical evolution can be used for this model too.

This model is specially suitable for studying the external shocks of the ejecta from the central source with disperse material or wind surrounding it, and/or the ISM. One expects that in these cases the density of the relativistic ejecta – the fast shell – be much higher than the wind or ISM and its extension much smaller. In Paper II we show that such a model along with a late emission from internal shocks can explain the shallow regime observed in the X-ray light curve of the majority of GRBs detected by Swift.

For studying the evolution of the active region, *a priori* we should also take into account the total size of the shells and the passage or coalescence time. However, observations show that synchrotron emission continues for a significant time after the end of the shock – when shells passed through each other or coalesced. For a far observer what is matter is the emission rather than physical encounter between shells. All these stages can be modelled by one of the models explained here or similar models for the evolution of r^0 . In this case the difference between various stages of the collision is reflected in the different value of parameters.

2.3 Evolution of relative Lorentz factor

To solve equation (26) we use a perturbative/iterative method based on the assumption that the dimensionless coupling in the r.h.s of this equation is smaller than one. By dividing both sides of (26) with $n_0 r_0^2$ one can extract the coupling A :

$$\frac{d}{d\left(\frac{r^0}{r_0^0}\right)} \left[\frac{\left(\frac{r^0}{r_0^0}\right)^3 + 1 + \frac{(3-D)n^0(r_0^0)}{N_0^0 r_0^0} \frac{r^0(r_0^0)}{r_0^0} \frac{0}{0} (1 - \frac{0}{0})}{(3-D)(1-0)} \right] = \frac{A}{r_0^0} \frac{r^0}{r_0^0} \left(\frac{r^0}{r_0^0}\right)^2 \quad (30)$$

$$A = \frac{4 m_p^2 \tau N_0^0 r^0(r_0^0)^2 e(r_0^0) B(r_0^0)}{3 m_e^2} \quad (31)$$

It is straightforward to see that if the initial column density of the slow shell/ISM $n_0^0 r^0(r_0^0) \cdot 10^{22} \text{ cm}^{-2}$, for any value of $e(r_0^0) < 1$ and $B(r_0^0) < 1$, the coupling $A < 1$. This upper limit on the shell column density is in the upper range of the observed total N_H column density of GRBs. However, the real N_H can be much higher than what is measured from the absorption of the soft X-ray at least ~ 100 sec after the trigger, because it is in conflict with N_H estimated from Lyman- α absorption (Watson et al. 2007). The difference can be due to the ionization of the neutral hydrogen by UV emission from the prompt emission. Nonetheless simulations of the formation of the electric and magnetic fields in the shocks show that the fraction of the kinetic energy transferred to the fields, specially to the magnetic field, is much less than one (Keshet et al. 2008). Therefore even with larger column densities, the value of A should be less than one and the validity of the perturbative method is justified.

The zero-order approximation corresponds to $A \ll 0$. In this case eq. (30) is a pure differential and its solution is trivial:

$$\frac{0}{(0)}(r^0) = \begin{cases} \frac{(3-D)^D}{\left(\frac{r^0}{r_0^0}\right)^3 + 1 + \frac{(3-D)^D}{0}} & \neq 3 \\ \frac{D}{\ln \frac{r^0}{r_0^0} + \frac{D}{0}} & = 3 \end{cases} \quad (32)$$

$$D = \frac{n^0(r_0^0) r^0(r_0^0) \frac{0}{0} \frac{0}{0}}{N_0^0 r_0^0} \quad (33)$$

where $\frac{0}{(0)}$ indicates the zero-order approximation for $\frac{0}{(r^0)}$. In the rest of this work we only concentrate on $\neq 3$, but calculations can be easily extended to this exceptional case.

The physical interpretation of (32) is quite evident. $\frac{0}{(r^0)}$ changes inversely proportional to the total mass of the shell including the accumulated mass of the swept material. This zero-order solution does not take into account the energy necessary to accelerate particles of the slow shell. Thus, its use without radiation corrections will lead to a violation of energy conservation. Parameter D presents the strength of the shock; smaller D , faster the constant term in the denominator becomes negligible with respect to radial growth and $\frac{0}{(0)}(r^0)$ approaches a cubic decline (for $= 0$) due to the adiabatic expansion. The origin of term (32) is partially geometrical and partially related to the density variation with r in the slow shell. It is the effective mass accumulation index of the shock.

As (32) is the dominant component of the dynamics and is used through out this work, it is useful to have its asymptotic behaviour for $\left(\frac{r^0}{r_0^0}\right) \ll 1$ and $\left(\frac{r^0}{r_0^0}\right) \gg 1$:

$$\frac{0}{(0)}(r^0) \sim \begin{cases} \frac{D}{3-D} \frac{0}{0} (1 - \frac{0}{D}) & \frac{r^0}{r_0^0} \ll 1 \\ (3-D) D \left(\frac{r^0}{r_0^0}\right)^3 & \text{For } \left(\frac{r^0}{r_0^0}\right)^3 > \frac{(3-D)^D}{0} \end{cases} \quad (34)$$

We use the zero-order solution in the r.h.s. of (30) to obtain the first-order correction of the solution. The n -order approximation corresponds to using the $(n-1)$ -order approximation in the r.h.s. of (30) and solving the equation:

$$\frac{\left(\frac{r^0}{r_0^0}\right)^3 + 1 + \frac{(3-D)n^0(r_0^0)}{N_0^0 r_0^0} \frac{r^0(r_0^0)}{r_0^0} \frac{0}{0} (1 - \frac{0}{0})}{(3-D)(1 - \frac{0}{(n)})} = \frac{A}{r_0^0} \frac{r^0}{r_0^0} \int_1^{\frac{r^0}{r_0^0}} \frac{0^6}{(n-1)} \frac{r^0}{x^2} dx \quad (35)$$

where $D_{(n)}$ is an integration constant. For any order of correction (35) must satisfy the initial condition i.e. $\frac{0}{(n)}(r_0^0) = \frac{0}{0}$ and from this constraint one can determine $D_{(n)}$. It is easy to see that $D_{(n)} = D$ for all orders of perturbation. Calling the integral term $M_{(n-1)}(r^0)$ for $(n-1)$ -order solution, we find the following recursive expression for $\frac{0}{(n)}$:

$$\frac{0}{(n)} = \frac{D}{\frac{1}{3} \left(\left(\frac{r^0}{r_0^0}\right)^3 + 1 + \frac{D}{0}\right)} \frac{A M_{(n-1)}(r^0)}{r^0(r_0^0)} \quad (36)$$

At this point we have to consider a model for r^0 . For the dynamical model $M_{(0)}$ becomes:

$$\begin{aligned} M_{(0)}(r^0) &= r_0^0 \left(\frac{0}{0}\right) \int_1^{\frac{r^0}{r_0^0}} \frac{0^{(0)}}{(1 - \frac{0}{(0)^2})^{\frac{1}{2}}} x^2 dx \\ &= \frac{r_0^0}{3} \left(\frac{0}{0}\right) (3-D)^{\frac{1}{3}} \int_0^{\frac{0}{(0)}(r^0)} dy \\ &= \frac{y^{3+\frac{1}{3}}}{(1-y^2)^{\frac{1}{2}}} \left(1 + \left(\frac{1}{(3-D)D} - \frac{1}{0}\right)y\right)^{-\frac{1}{3}} \end{aligned} \quad (37)$$

The second form of the integral is obtained using $r_0^{(0)}$ solution. Unfortunately this integral can not be determined analytically. Nonetheless, by expanding one of the two terms in the integrand it is possible to find an approximation which is useful for getting an insight into the behaviour of $r_0^{(1)}$, its dependence on various parameters, and the importance of radiation correction. They are summarized in Appendix A.

For quasi-steady model $M_{(0)}(r^0)$ is:

$$M_{(0)}(r^0) = r_1^0 \int_1^{\frac{r^0}{r_0^0}} \frac{x^2 (1 - \frac{x}{r_0^0})}{(1 - \frac{x}{r_0^0})^3} dx = \frac{r_1^0}{3} ((3 - D)^{\frac{1}{3}} - \int_0^{\frac{r^0}{r_0^0}} dy) \frac{y^{\frac{1}{3}-3}}{(1 - \frac{y}{r_0^0})^3} (1 + (\frac{1}{(3-D)} - \frac{1}{r_0^0})y)^{\frac{1}{3}-3} \left[1 - ((3-D)^{\frac{1}{3}} - (1 + (\frac{1}{(3-D)} - \frac{1}{r_0^0})y)^{\frac{1}{3}-3}) \right] \quad (38)$$

The similarity of the second term in (38) to the integrand of (36) shows that at first order of radiative correction the two terms in (28) act independently. The constant term leads to the first term in (38) which is equivalent to (36) with

$\ell = 0$, i.e. an active region with constant thickness. The term proportional to $(r_0^0 - r^0)$ in (28) is responsible for the second term in (38). Up to a constant it is also the expression for a constant thickness model with $\ell = 0$. This means that the effect of power-law term in (28) is very similar to power-law dependence of fields and shell density on r^0 . This behaviour justifies the name quasi-steady we have given to this model. Analytical approximations of these integrals can be found in Appendix A.

In the last paragraph we considered power-law dependence on r^0 for the electric and magnetic fields. The case of an exponential rise or fall of the fields is important at the beginning and at the end of gamma-ray spikes or early X-ray arcs. For this case, the only modification in (37) and (38) is the replacement of x with $\exp(-x)$ where here is a dimensionless coefficient determining the speed of exponential variation. It is negative for rising fields and positive when fields are declining, similar to the power-law case. In the same way if the electron distribution $n_e(r)$ includes an exponential cutoff (Dempsie & Dwyer 2007), an exponential term similar to the term for fields appears in the expression for $M_{(0)}(r^0)$. Therefore in a general case, the integrand in (37) and (38) includes an exponential term which makes it even more complex. Nonetheless, the expansion of the exponential permits to obtain the analytical approximation given in the Appendix A.

Finally by using $M_{(0)}(r^0)$ in (36) and (9), we can determine $r_0^{(1)}$ the first-order radiation corrected evolution of $r_0^{(0)}$ and column density $n_0^{(0)}(r^0) r^0$ with radius/time. The complexity of expressions for $M_{(0)}(r^0)$ and consequently for $r_0^{(1)}$ does not permit to investigate the effect of various quantities from the exact calculations and we leave this for Paper II where we numerically evaluate the behaviour of shocks kinematic and radiation. Here we just consider the simplest cases when in (34), $r^0 = r_0^0$ & 1 or $r^0 = r_0^0 (3 - D)^{\frac{1}{3}}$. Using (A6) and (A7) respectively for large and small ℓ , we

find following expressions for $M_{(0)}(r^0)$ when $\ell = 1$:

$$M_{(0)}(r^0) = r_0^0 B (1 - \frac{1}{C}) (1 + (3 - \frac{2}{3}) \frac{r_0^0}{r^0})^{\frac{1}{3}} \quad \text{for } j \neq 0 \quad (39)$$

$$M_{(0)}(r^0) = r_0^0 B \left[(3 - D) \left(2 + \frac{1}{3} \right) + \frac{r_0^0}{r^0} \left(\frac{(3 - D) (3 - \frac{2}{3}) (1 + \frac{1}{3})}{(1 + \frac{1}{3})} \right) \right] \quad \text{for } j \neq 0 \quad (40)$$

$$B = \frac{r_0^0}{(3 - D)^{\frac{1}{3}}} C^{\frac{1}{3}}; \quad C = \frac{(3 - D) D}{r_0^0} \quad (41)$$

Therefore $M_{(0)}(r^0) / r_0^0 B \approx 1$ for $\ell = 1$. The constant coefficient is expected to be of order 1. By applying these results to (36) we find:

$$r_0^{(1)} = \frac{D}{r_0^0} + \frac{A B^0}{(1 - A B^0)} \quad (42)$$

where B^0 is B multiplied by the corresponding constant coefficients in (39) or (40) depending on the value of ℓ . Comparing this result with the corresponding $r_0^{(0)}$ we conclude that the strength of the radiation correction of $r_0^{(0)}$ and its effect on the kinematic of the ejecta/jet depends on $S = A B^0$. As B^0 is proportional to $D^{-\frac{1}{3}}$, for a positive ℓ and same A , larger D (stronger shock), smaller S . In this case the kinetic energy of the shock is much larger than radiation and therefore the synchrotron emission does not significantly modify the evolution of the shock. Note also that although S is linearly proportional to the synchrotron total coupling A , it depends non-linearly on D through a power which depends on the time/radius variation of the electric and magnetic fields as well as the density of the shells. The quantity S in this model depends also on r_0^0 : larger r_0^0 , larger the influence of radiation. This simply means that the effective thickness of the active region decreases faster when the effect of radiation is stronger. This behaviour is consistent with the phenomenology of the model described here.

Similar expressions can be found for the other extreme case i.e. when $r^0 = C r_0^0$ $\ell = 1$:

$$M_{(0)}(r^0) = \frac{r_0^0}{r^0} \frac{C^{\frac{1}{3}} (1 - \frac{1}{C})}{(3 - D)^{\frac{1}{3}}} \left\{ \left[\frac{1}{1 + \frac{1}{3}} + \frac{(3 - \frac{2}{3})^{\frac{1}{3}}}{1 + \frac{1}{3}} \right] \left(\frac{C r_0^0}{r^0} \right)^{\frac{1}{3}} \left[\frac{1}{1 + \frac{1}{3}} + \frac{(3 - \frac{2}{3})^{\frac{1}{3}}}{1 + \frac{1}{3}} \right] \left(\frac{C r_0^0}{r^0} \right)^{\frac{2}{3}} \right\} \quad \text{for } j \neq 0 \quad (43)$$

$$M_{(0)}(r^0) = \frac{r_0^0 C^1}{(3)^0} \left(1 + \frac{1}{C}\right) \left\{ \left[1 + \frac{(3)^0}{3} + \frac{(1)^0}{3} \left(1 + \frac{(3)^0}{3} + \frac{(1)^0}{3}\right)\right] \left(\frac{Cr_0^3}{r^3}\right)^{2+\frac{1}{3}} \right. \\ \left. + \frac{(3)^0}{3} \left(\frac{Cr_0^3}{r^3}\right)^2 + \frac{Cr_0^3}{3} \left(1 + \frac{1}{C}\right) \left(1 + \frac{(3)^0}{3} + \frac{(1)^0}{3} \left(1 + \frac{(3)^0}{3} + \frac{(1)^0}{3}\right)\right) \right\} \\ \text{for } j \neq 0 \quad (44)$$

When $r^0 = Cr_0^0 \neq 0$, $M_{(0)}(r^0) \neq \text{const.}$, if $2 + \frac{1}{3} > 0$ for $j \neq 0$ or $1 + \frac{1}{3} > 0$ for $j = 1$. This can be interpreted as a saturation state for the synchrotron radiation which has been observed specially in bright bursts where peaks of the prompt gamma-ray emission are roughly square-like. Examples are GRB 060105 (Ziaeepour et al. 2006a), GRB 061007 (Schady et al. 2006b, 2007), GRB 060813A (Moretti et al. 2006), and GRB 070427 (Sato et al. 2007a). Even the Super Burst GRB 080319B (Racusin et al. 2008a,b) seems to consist of 3 overlapping square shape peaks. See also simulations in Paper II.

The conditions mentioned above can be considered as consistency conditions because if they are not satisfied $M_{(0)}(r^0) \neq 1$ which is not physically acceptable. Therefore these conditions constrain parameters of the model α , β , and γ . For instance, for a slow shell with a roughly constant density $\rho = 0$. Therefore α depends only on the behaviour of electric and magnetic fields. If the variation index of these fields are small and positive, the value of α can be small, i.e. the radiation will not vary very quickly. By contrast, a negative index - increasing fields - can not last for long time and imposes a large value for α . This simple argument shows that there is an intrinsic relation between these parameters. However, only a detailed modelling of the microphysics of the shock will be able to determine possible relations and their physical origin. Nonetheless the discussion above shows that the simple model studied here is consistent and includes some of the important properties of the phenomena involved in the production of GRBs.

Using (36) one can see that a constant $M_{(0)}(r^0)$ is equivalent to redefinition of D . Therefore when the radiation term arrives to its maximum, ρ^0 evolution becomes like a non-radiating ejecta.

In the case of a quasi-steady active region, the behaviour of $M_{(0)}(r^0)$ is essentially similar because of similarity between two models explained above. However, the time scales and indexes are different. For instance, when $\alpha = 1$ the value of $M_{(0)}(r^0)$ is proportional to ρ^0 with a coefficient equal to (39) or (40) and $\beta = 0$, minus the same term with $\alpha = 1$. In this case, the initial ρ^0 does not have an explicit contribution and the slope of $M_{(0)}(r^0)$ is smaller than dynamical model. For $r^0 = Cr_0^0 = 1$ if other parameters are the same as dynamical model, the absence of ρ^0 and smaller power of $Cr_0^0 = r^0$ means that $M_{(0)}(r^0)$ approaches its maximum value slower. There is also a slower change when one of the two contributor terms becomes too small and negligible. As expected, all these properties make this model more suitable for modelling the afterglow.

Up to now we have only discussed the solutions of dynamical equation (26) corresponding to the rise of the synchrotron emission. The falling edge of the emission i.e. when $M_{(0)}(r^0) \neq 0$ can be obtained simply by time/radius reversal of rising solutions, see eq. (29). For instance in (39) and (40) if $r^0 < r_0^0$, $\alpha < 0$. By moving the initial condition from r_0^0 to r^0 , we obtain a positive but decreasing value for $M_{(0)}(r^0)$ which becomes zero at $r^0 = r_0^0$. These approximations however do not permit to determine when the radiation begins to decrease. For this we need a detailed study of the evolution of fields and other shock properties.

In summary, the evolution of ρ^0 determines the kinematic of the burst and is important for the estimation of all observables such as what we will discuss in the next sections - synchrotron flux, hardness ratios, etc. ρ^0 is also important for determining the evolution of other parameters that are not directly observable and a model must be used for their extraction from data. A good example is the time variation of ν_m^0 the minimum characteristic frequency of the synchrotron emission. It determines the behaviour of the spectrum and light curves (see expression (78) below for its definition). Assuming the simplest case of $n_a^0 = n_0^0$ in (15), from the definition of ν_m^0 one can see that ν_m^0 / ω_B . The proportionality coefficient is time/radius independent.

2.4 Synchrotron flux and spectrum

In this section we first remind the synchrotron emission for the purpose of completeness and then we use the results for determination of lags between the light curves of different energy bands.

The ejecta from a central engine that produces the gamma-ray burst is most probably collimated and jet-like, otherwise the observed energy is not explainable. On the other hand for the far observers, even a spherical relativistic emission looks collimated to an angle $\theta < 1 = \gamma$ along the line of sight where γ is the Lorentz factor of the emitting matter in the observer rest frame (Rees 1967). Therefore in any case we need to consider the angular dependence of the synchrotron emission. Moreover, we need to consider the delay as well as angular dependence of the Doppler shift of the emission. Simulations show that even with an angular independent emission, these effects can a priori explain the lag between different bands observed in both BATSE and Swift bursts (Qin 2002; Qin et al. 2004; Lu et al. 2006). However, in these simulations the spectrum and the time profile of emission have been put by hand.

There are a number of evidence against a high latitude/Doppler effect origin of the observed lags. First of all the total effect of high latitude emission decreases when Lorentz factor is very high. It is expected that in GRBs $\gamma \sim 100$, and therefore this effect should be very small. In addition, even in the early X-ray emission where it was expected that this effect dominates, it has not been observed. On the other hand, for a given category of bursts, short or long, it does not seem that there is any relation between lags and spectrum as expected from a Doppler effect. Therefore we conclude that the contribution of high latitude emission and Doppler effect is sub-dominant and can not explain the observations. On the other hand, we show that even with neglecting the high latitude emission, due to the evolution

of physical properties a lag between different energy bands exists.

In the model presented here the synchrotron emitting matter is confined to the active region. Therefore we identify the bulk Lorentz factor with respect to the observer with the average Lorentz factor of the active region with respect to the observer. It can be related to the relative Lorentz factor $\gamma^0(r^0)$ obtained in Sec. 2.2 and the final Lorentz factor when two shells are coalesced:

$$\gamma(r) = \gamma_f^0(r) (1 + \gamma_f^0(r)) \quad (45)$$

where γ_f is the Lorentz factor of coalesced shells with respect to observer. The initial value of $\gamma^0(r)$ is the relative Lorentz factor of the colliding shells. In the case of an external shocks on a low velocity surrounding material or the ISM $\gamma_f \approx 1$ and $\gamma(r) \approx \gamma^0(r)$. Note that here we have written with respect to observer coordinate r because on what concerns the synchrotron emission, only the observations of far observers matter.

The energy (intensity) angular spectrum of synchrotron emission (Jackson 2001) by one electron or positron in a frame where it is accelerated to a Lorentz factor of γ_e is⁵:

$$\frac{d^2 I^0}{d\Omega d\gamma^0} = \frac{3e^2 \gamma_e^2}{4 \gamma_e^2 \gamma_c^2 c} (1 + \gamma_e^2 \gamma_c^2)^2 \left[K_{2/3}^2(\gamma_e^2 \gamma_c^2) + \frac{\gamma_e^2 \gamma_c^2}{1 + \gamma_e^2 \gamma_c^2} K_{1/3}^2(\gamma_e^2 \gamma_c^2) \right] \quad (46)$$

$$\gamma_c^0 = \frac{3}{2} \gamma_e \left(\frac{c}{v_0} \right) = \frac{3e^2 B^0}{2cm_e} \quad (47)$$

$$\frac{\gamma_e^0}{2 \gamma_c^0} (1 + \gamma_e^2 \gamma_c^2)^{3/2} \quad (48)$$

Quantities with a prime in (46) to (48) are with respect to the frame where Lorentz factor of electrons is γ_e . Here we identify this frame as the rest frame of the active region. γ^0 is the Larmor radius of electrons. The angle θ^0 is the angle between acceleration direction and emission. Without loss of generality it can be assumed to be in x-z plane. Therefore $d\Omega = \sin\theta d\theta d\phi$ (Jackson 2001). When $\theta \ll 1$, $d\Omega \approx d\theta d\phi$.

To obtain the power spectrum that is the measured quantity, we must divide the intensity by the precession period of electrons $2\pi/\omega_c = c/v_e$. We expect that accelerated electrons have a range of Lorentz factors, therefore we should also integrate over their distribution:

$$\frac{d^2 P^0}{d\Omega d\gamma^0} = \frac{e^2}{4 \gamma_c^3 c} \int_{\gamma_{\min}}^{\gamma_{\max}} d\gamma_e n_e^0(\gamma_e) \gamma_e^{-1} \left(\frac{\gamma_e^0}{\gamma_c^0} \right) (1 + \gamma_e^2 \gamma_c^2)^2 \left[K_{2/3}^2(\gamma_e^2 \gamma_c^2) + \frac{\gamma_e^2 \gamma_c^2}{1 + \gamma_e^2 \gamma_c^2} K_{1/3}^2(\gamma_e^2 \gamma_c^2) \right] \quad (49)$$

Note that we have divided the angular power spectrum by γ_e^0 to make it dimensionless. In the observer's rest frame the spectrum is transferred as (Sadun & Sadun 1991;

Huang et al. 2000; van Eerten & Wijers 2009):

$$\frac{d^2 P}{d\Omega d\gamma} = \frac{1}{\gamma^2 (1 - \cos\theta)} \frac{d^2 P^0}{d\Omega^0 d\gamma^0} \quad (50)$$

$$\gamma = \frac{\gamma^0}{(1 - \cos\theta)} \quad (51)$$

$$\cos\theta = \frac{\cos\theta^0 + \gamma^0}{1 + \gamma^0 \cos\theta^0}; \quad \cos\theta^0 = \frac{\cos\theta}{1 - \gamma \cos\theta} \quad (52)$$

where in equations (50) to (52), γ is related to the Lorentz factor of the active region with respect to the observer. To find the total power at a given frequency $P(\nu; \theta)$ in the frame of a far observer, we integrate over the distribution of accelerated electrons and the emitting volume but constrain it to the emission in the direction of the observer. As we assumed that the active region is thin, we neglect the absorption of synchrotron photons inside the active region itself. Without loss of generality we put the observer at $\theta = 0$. In this case for an electron moving at angle θ^0 with respect to observer, only photons emitted in the direction of $\theta^0 = \theta^0_1$ are detected by the observer. Therefore we need to integrate either on θ^0_1 (or equivalently θ^0_1) or on $\theta^0(\theta)$. For simplicity of notation we use the latter. As the synchrotron angular distribution does not depend on θ (or θ^0) we only need to integrate over θ^0 (or equivalently θ^0_1):

$$\frac{dP}{d\Omega} = 2 \int_{r_{\min}}^{r_{\max}} dr \int_{\theta_{\min}}^{\theta_{\max}} d\cos\theta \frac{d^2 P(\nu; \theta; \theta^0)}{d\Omega d\gamma} \quad (53)$$

θ_{\min} and θ_{\max} are minimum and maximum visible angle for the observer with the constraint $|\theta_{\min}| < \pi/2$ and $|\theta_{\max}| < \pi/2$. We define $\theta_{\max} + \theta_{\min} = \pi/2$ as the view angle of the observer with respect to the ejecta/jet axis. These angles are not directly measurable and therefore the simplest assumption is a symmetric ejecta $\theta_{\max} = \theta_{\min} = \pi/2$, i.e. $\theta = 0$. Note that photons coming from $\theta \neq 0$ arrive to the observer with a time delay t where $t(\theta)$ is (Rybicki & Lightman 2004):

$$t(\theta) = \frac{r(1 - \cos\theta)}{c(r)(1 + \gamma^2 \sin^2\theta)^{1/2}} \quad (54)$$

In (54) we have assumed that the initial radius from which the shells are ejected from the central engine is much smaller than their distance from it when they collide. Therefore, the initial radius is neglected. Due to the direct relation between radius and time in this model, $t - t(\theta)$ can be replaced by $r(\theta) = r - c(r)t(\theta)$. The quantity $r(\theta)$ should not be confused with the thickness of the active region r .

In this model we have considered r and the physical properties of the active region are close to uniform. Thus, the integral over the interval r and $r + r$ becomes trivial if we consider r to be the average distance of the active region. This is similar to the way we calculated kinematic quantities in Sec. 2.2. With this simplification the total spectrum becomes:

$$\frac{dP}{d\Omega} = 2 \int_{r_{\min}}^{r_{\max}} dr \int_{\theta_{\min}}^{\theta_{\max}} d\cos\theta \frac{d^2 P(r - r(\theta); \theta; \theta^0)}{d\Omega d\gamma} \quad (55)$$

If we use (7) to describe r as a function of time, equation (55) depends only on t and θ .

The width r can in general depend on the energy. In Sec. 2.1 we described that when electrons lose their energy,

⁵ The expression (46) is valid for small θ^0 angles. However, the main part of the emission is in $\gamma_e^0 < 1$, and the intensity exponentially decreases for $\gamma_e^0 \gg 1$. Therefore it is a good approximation for any angle (Jackson 2001).

they get distance from the shock front or in another word are pushed to the upstream. Although in this region the magnetic field is expected to be weaker, it can be enough for the low energy emissions, UV, optical, IR. Moreover, in a collimated or structured jet⁶ these less accelerated particles emit mostly in lower energies. In this simple model of shock one way of taking into these effects is to consider that r as well as r_{min} and r_{max} depend on the energy. For r we can simply assume that r_0 in dynamical model or r_1 in the quasi-steady model are energy dependent. Estimation/modeling of energy dependence of r_{min} and r_{max} is more difficult because the only way to modify them is through β . Assuming $\beta_{\text{jet}} > 1$ we must consider that β is γ -dependent. This needs a modification of the dynamics and makes the model too complicated. For this reason here we ignore the energy dependence of opening angle of the jet.

The differential term in (55) can be replaced by (50) and (49). We must also take into account the proper time delay discussed above. Therefore:

$$\frac{dP}{d\epsilon} = \frac{e^2}{2} r^2 \left(\frac{\epsilon^0}{\epsilon_{\text{cc}}^0} \right) \int_{r_{\text{min}}}^{r_{\text{max}}} d \cos \left[\frac{r(1 - \cos \theta)}{(1 + \frac{1}{2} \sin^2 \theta)^{1/2}} (1 - \beta(t) \cos \theta) \right] \int_{\theta_{\text{min}}}^{\theta_{\text{max}}} d \theta \frac{n_e^0(\epsilon)}{\epsilon^3} (1 + \frac{1}{2} \beta^2)^2 \left[K_{2=3}^2(\theta) + \frac{\frac{1}{2} \beta^2}{1 + \frac{1}{2} \beta^2} K_{1=3}^2(\theta) \right] \quad (56)$$

$$\epsilon_{\text{cc}}^0 = \frac{\epsilon^0}{\epsilon} = \frac{3eB}{2m_e} \quad (57)$$

As the angle θ and therefore the delay is small, we use Taylor expansion around r to obtain the explicit expression for \cos in the integrand of (56):

$$\left(\frac{r(1 - \cos \theta)}{(1 + \frac{1}{2} \sin^2 \theta)^{1/2}} \right) (r) (1 - \beta(t) \cos \theta) \approx \frac{r(1 - \cos \theta)}{(1 + \frac{1}{2} \sin^2 \theta)^{1/2}} \frac{d(r)}{dr} + \dots \quad (58)$$

In a similar way we can expand $\beta(t; \epsilon)$ around r :

$$\left(\frac{r(1 - \cos \theta)}{(1 + \frac{1}{2} \sin^2 \theta)^{1/2}} \right) (r) (1 - \beta(t) \cos \theta) \approx \frac{r(1 - \cos \theta)}{(1 + \frac{1}{2} \sin^2 \theta)^{1/2}} \frac{d(\beta(t))}{d\epsilon} + \dots \quad (59)$$

As $\sin \theta \approx \theta$, we can also expand the γ -dependent terms in (58) and (59). It is more convenient to use the relation between γ and ϵ^0 in (52) and transfer to ϵ^0 . We keep only terms up to β^2 order. With these simplifications

the total energy spectrum can be written as:

$$\frac{dP}{d\epsilon} = \frac{e^2}{2} r^2 \left(\frac{\epsilon^0}{\epsilon_{\text{cc}}^0} \right) \frac{r}{(r)} \int_{r_{\text{min}}}^{r_{\text{max}}} d \cos \theta \left(1 + G(r) \beta^2 + \dots \right) \int_{\theta_{\text{min}}}^{\theta_{\text{max}}} d \theta \frac{n_e^0(\epsilon)}{\epsilon^3} (1 + \frac{1}{2} \beta^2)^2 \left[K_{2=3}^2(\theta) + \frac{\frac{1}{2} \beta^2}{1 + \frac{1}{2} \beta^2} K_{1=3}^2(\theta) \right] \quad (60)$$

$$G(r) = \frac{\beta^2(r) (1 - \cos \theta)}{2(1 + \cos \theta)} \left(\frac{\epsilon^0}{\epsilon_{\text{cc}}^0} \frac{\epsilon^0(r)}{\epsilon^0} + \frac{1}{D} \right) \left(\frac{\beta}{1 + \beta \cos \theta} \right)^2 \quad (61)$$

The coefficient $G(r)$ in (60) presents the lowest order correction due to the Doppler effect and delay of high latitude emissions. As expected, for $\beta \ll 1$, $G(r) \approx \beta^2 \ll 0$. Moreover, $G(r)$ does not depend on ϵ^0 (or equivalently ϵ), and therefore it does not affect the lag between different energy bands itself.

Apart from the energy dependence of r , r_{min} , and r_{max} mentioned before and has an intrinsic origin, i.e. are related to the evolution of the active region and the structure of the jet/ejecta, there are two other effects that can create a lag: angular dependence of the emission and time/radius dependence of β and ϵ_{cc}^0 . Assuming a homogeneous density for the colliding shells, equation (15) shows that the time dependence of β is mainly due to variation of the relative Lorentz factor γ and the electric field energy fraction index ϵ with time. The variation of ϵ_{cc}^0 is also possible if the magnetic field changes with time. If fields are considered to be constant during the emission – as it is the case for many GRB models in the literature – only dynamical friction and decrease in β remain. They may be insufficient to explain the observed lags because the Doppler and high latitude correction is usually small, specially when β is large. In fact simulations show that with an angular independent emission flux, large lags can be obtained only if the emission happens at large radius with respect to the central engine, $> 10^{15}$ cm (Lu et al. 2006). This is orders of magnitude larger than what is expected from internal shocks. As synchrotron emission is highly angular dependent, lags are expected not only from Doppler and high latitude correction but also when these effects are ignored. In fact this can be seen in (60). The integration over θ can be expressed as $f(\beta)$ where β is defined in (48) for $\epsilon = \epsilon_{\text{min}}$. It is then clear that r and ϵ^0 dependence of the integrand are not factorisable, and therefore even when $G(r)$ is ignored, the r dependence of $dP/d\epsilon$ can not be factorized. Therefore, giving the expectation of high collimation and large Lorentz factor, the main cause of the observed lags in the GRBs seems to be the time variation of physical properties of the active region such as r , β , and electric and magnetic fields.

We note that the zero-order term in (60) is the same as the expression (49) for the synchrotron emission by one particle. Therefore, for this part of integration in (60) we can use the well known expression for the spectrum (Schwinger 1949; Westfold 1959; Jackson 2001; Rybicki & Lightman 2004). For determining the Doppler and high latitude correction

⁶ A structured jet is usually considered to have a transverse gradient in density (Xu et al. 2005; Takami et al. 2007). However it is expected that gradually a transverse gradient in Lorentz factor forms too.

term we can again use the integration method used for the zero-order term and express (60) as a sum of Bessel functions (Westfeldt 1959). Finally we find the power spectrum with the first order correction for Doppler effect and high latitude delays⁷:

$$\begin{aligned} \frac{dP}{!d!} = & \frac{P}{3} \frac{3e^2}{r^2} \frac{r}{(r)} \int_m^1 d_e n_e^0(e_e) e_e^{-2} \\ & \left\{ 2 \int_{\frac{1}{10}}^1 K_{5=3}(\gamma) d\gamma + \frac{7}{12} G(r) \left(\frac{1}{10} \frac{cc}{10} \right) \right. \\ & \left[\frac{22}{7} K_{1=3} \left(\frac{1}{10} \frac{cc}{10} \right) - 9 \left(\frac{1}{10} \frac{cc}{10} \right) K_{2=3} \left(\frac{1}{10} \frac{cc}{10} \right) + \right. \\ & \left. \left. 3 \left(\frac{1}{10} \frac{cc}{10} \right) \int_{\frac{1}{10}}^1 K_{5=3}(\gamma) d\gamma \right] \right\} \end{aligned} \quad (62)$$

We can further integrate (62) if we consider a specific distribution for accelerated electrons $n_e^0(e_e)$. In Appendix B we calculate $dP=!d!$ for the power-law distribution (13) and comment the case for a power-law with an exponential cutoff distribution. Here we use those results to discuss the lowest order properties of the spectrum and light curves.

2.5 Lag between light curves

The presence of a lag between various energy bands of the GRBs has been detected in BATSE (Kouveliotou et al. 1993) and INTEGRAL (Foley et al. 2008) light curves and confirmed by Swift-BAT (Sakamoto et al. 2007). Observations show that in most long bursts there is a significant lag – from tens to few hundreds of milliseconds between soft and hard bands. By contrast, in short bursts the lag is very small and within the present sensitivity and time resolution of gamma-ray telescopes it is consistent with zero or at most a few milliseconds. These two classes are respectively associated with the explosion of massive stars (collapsars, hypemova) and to the merging of two compact objects – a neutron star with a black hole, two neutron stars, or a neutron star and a white dwarf. There is however evidence for the difference between lags of the separate peaks in the same burst. Moreover, some bursts that according to their T_{90} can be classified as short such as GRB 080426 (Ziaeeipour et al. 2008b) have relatively long lags of few tens of milliseconds. On the other hand some apparently long bursts such as GRB 060614 (Mangano et al. 2007) and GRB 080503 (Mao et al. 2008) have small lags similar to the short bursts. Various explanations have been put forward for these out of normal behaviours: sensitivity of detectors only to the peak of a long burst leading to its misclassification as short, existence of a separate class of GRBs with intermediate durations and lags, long tail emission in otherwise short burst for bursts with long T_{90} and small lags. Some authors even rule out the association of long GRBs – hypemova, short GRBs – collision of compact objects, and suggest that they should be classified according to their lags: Short lags old population, long lags young population (Zhang et al. 2007a). A part from

classification of progenitors of the GRBs, lags along with luminosity have been also used as proxy for the GRBs redshift determination (Norris et al. 2000).

In summary, lags seem to be important quantities related to the nature of central engine of the GRBs, properties of the ejecta, and the surrounding material. They can be relatively easily measured, and therefore it is important to be able to relate them to these phenomena. Some authors have tried to explain lags just as a geometrical effect related to the high latitude emission and associated Doppler shift (Qin 2002; Qin et al. 2004; Lu et al. 2006). As we have discussed in the previous section and also regarding r and $!$ dependence of the spectrum in (62), it is evident that even without Doppler shift and high latitude corrections the r dependence – equivalent to time dependence in the model discussed here – and $!$ dependence are not factorisable, and therefore light curves in different energy band can not be the same even when they are normalized to smear the amplitude difference.

To define and determine lags we need fast varying features such as peaks. In the gamma-ray bursts light curves peaks are mostly observed in the prompt gamma-ray energy bands. Nonetheless, fast slew of the Swift satellite and some of the ground based robotic telescopes have permitted to observe the counterpart peaks or at least evidence of their presence in X-ray and optical bands. A realistic model for the lags should be able to predict the lag in all these energy bands if they have the same origin. On the other hand, a deviation of some bands from predictions can be used as an evidence for a different origin of the corresponding feature.

The nature of peaks and their profile are not well understood. In the framework of the synchrotron emission from internal shock model as the origin of the prompt gamma-ray emission, the rising side of a peak indicates the beginning of the collision between shells and formation of the electric and magnetic fields that leads to the acceleration of charged particles and synchrotron emission in the induced magnetic field. Decreasing edge corresponds to the separation and/or the total coalescence of the shells. However, it is expected that even before separation/coalescence, microphysics in the active region arrive to a roughly steady state during which only slight changes due to e.g. density fluctuation in the shells will occur. In particular when the initial evolution of the microphysics is much faster than the time of the passage of the shells through each other we expect that for a limited duration the active region has quasi-steady characteristics. Assuming such a case – in accordance with the discussion about the evolution of r in Sec. 2.2 – a peak corresponds to:

$$\frac{d}{dt} \left(\frac{dP}{!d!} \right) = c(r) \frac{d}{dr} \left(\frac{dP}{!d!} \right) = 0 \quad (63)$$

The lag for a given peak corresponds to the difference between peak time/radius for two frequencies or two energy bands. Usually observations are performed in known energy bands. Therefore, the purpose of the lag measurement is to determine the difference between r_{peak} the solution of equation (63), at two different energies. In the rest of this section we use the results of Sec. 2.4 to determine the lags. Using (62) the peak equation (63) can be written as a

⁷ For simplifying the integration over $!$ in (60), we consider $\cos^0 + \frac{1}{2}$. This is a valid approximation when $! \rightarrow 1$ and $!$ is independent of the synchrotron emission.

a strong apparent collimation of the radiation from a spherically symmetric ejecta to angles $\theta < \theta_{\text{boost}} = 1/\gamma$ for a far observer (Rees 1967). It is also possible that the ejecta is not intrinsically spherical but jet like (Rees et al. 1998). In this case after deceleration of the jet during its propagation through the surrounding material or the ISM, at some radius/time $\theta_{\text{boost}} > \theta_{\text{open}} = \theta_{\text{max}} - \theta_{\text{min}}$ and radiation is no longer collimated. This leads to a drop of observed flux (Sari et al. 1999). As this effect is purely kinematic/geometric it should not depend on energy. Observations of the Swift and robotic ground telescopes however contradict this expectation. The breaks seen in the afterglow light curves are usually chromatic. In many bursts no optical break has been observed up to millions of seconds after the prompt emission (Roming et al. 2008). In some bursts, mostly bright ones but not always, no break has been observed in X-ray either (Sato et al. 2007b). In a significant fraction of bursts multiple breaks in the X-ray light curve have been observed. A priori only one of these breaks (if any) can be due to the jet break. Therefore, the mechanism of break is more complex than just a kinematical effect. Here we want to argue that even in the simple case of the opening due to deceleration, we should not expect to have an achromatic break if the afterglow is a synchrotron radiation.

For obtaining the analytical expression (62) for the radiation spectrum, we made the simplifying approximation that $j_{\text{min}} = j_{\text{max}} - 1$. This permitted to analytically integrate the angular integral in (60). Without this approximation (60) depends on the opening angle. The justification for this approximation was that the synchrotron emission is highly directional and for $\gamma \gg 1$ the intensity reduces exponentially because the value of $\sin \theta$ in the integrand of (60) grows. γ increases with energy and therefore high energy photons are preferentially emitted at small angles with respect to electrons boost direction. When the collimation is reduced, the observer receives less high energy photons from high latitude electrons (Panaitescu & Meszaros 1998) and therefore the effect of the jet break in uences high energy light curves earlier than low energy ones. Conceptually this effect is very similar to the lag between light curves. It is however more difficult to investigate it mathematically because the angular integral (60) can not be determined analytically as explained above.

On the other hand, it is not sure that the reduction of Lorentz factor can explain the absence of a break in optical frequencies when it is observed in X-ray. A number of suggestions have been put forward to explain observations (Panaitescu 2005; Misra et al. 2007). In the framework of the model presented here it can be at least partly explained by the energy dependence of the geometry of the active region. In fact the material that has lost its energy and has been decelerated is pushed behind the front edge of the shock. Due to the scattering it also has a relatively larger transverse momentum (See simulations in (Vigeli et al. 2007) for non-relativistic shocks). Thus, less boosted particles in the ejecta have intrinsically a larger opening angle. This leads to a later jet break for the softer photons originating in this extended region. Therefore one does not need additional processes (Rees & Meszaros 1998; Sari & Meszaros 2000), energy (Dai & Lu 1998; Rees & Meszaros 2000; Zhang & Meszaros 2002) and/or components (De Pasquale et al. 2008) to explain the breaks.

The complex geometry of matter and fields in the material and shock can explain apparently contradictory observations. As for multiple breaks, they can be due to the fact that multiple shells are ejected by the central engine. This is in the same spirit as the structured jet models (Xu et al. 2005; Takami et al. 2007). If they do not completely coalesce both the tail emission and the afterglow due to the external shocks will combinations of radiation from separate remnant shells. In this case the break of radiation from each shell is independent of others and a far observer who detects the total emission will observe multiple breaks in the emission.

3 EXTRACTION OF PARAMETERS FROM DATA

The model described in the previous sections has a large number of parameters. It would not help to better understand the physics of gamma-ray bursts production and their engine if we can not estimate the parameters of this or any other model from data. On the other hand, the only conveyor of information for us is the emission in different energy bands. Therefore, we must find the best ways to extract the information as efficient as possible. In this section we suggest a procedure for extracting the parameters of the model. We also discuss their degeneracies.

Since the massive detection of GRBs by BATSE, many efforts have been concentrated to understand their spectrum. However, very little information could be extracted from the spectra. The complexity of time and energy dependence of the spectrum (62) explains why the time averaged spectrum does not carry extractable information. As GRBs evolve very quickly both in time and in energy, integration over these quantities smears the useful information. Unfortunately the effective detection surface of present gamma-ray detectors is too small and we do not have enough photons to make a broad spectrum in small time intervals. In this situation hardness ratios and their time variation are more useful quantities. Therefore we first discuss what we can extract from hardness ratios.

Consider a power-law distribution for electrons, equation (B1) shows that at a given time the spectrum can be expanded as a power of $\gamma_m^0 = \gamma_{\text{cc}}^2 \gamma_m^{-2}$. The coefficient in front of the integral term does not depend on energy. Therefore, if we neglect $G(r)$ i.e. assuming the bulk Lorentz factor is very large, the hardness ratios depend only on the integral determined in (B4). We define the hardness ratio between two bands with logarithmic mean energies ϵ_1 and ϵ_2 as:

$$H R_{12}(r) = \frac{\int_{\epsilon_1}^{\epsilon_2} d\epsilon \frac{dP}{d\epsilon}}{\int_{\epsilon_1}^{\epsilon_2} d\epsilon \frac{dP}{d\epsilon}} \bigg|_{\epsilon=\epsilon_1}^{\epsilon=\epsilon_2} \quad (76)$$

$$\frac{\int_{\epsilon_1}^{\epsilon_2} d\epsilon \frac{dP}{d\epsilon}}{\int_{\epsilon_1}^{\epsilon_2} d\epsilon \frac{dP}{d\epsilon}} \bigg|_{\epsilon=\epsilon_1}^{\epsilon=\epsilon_2} \quad (77)$$

The approximations for integrals are valid when $\epsilon_1 = \epsilon_2$. Expression (B4) shows that at a constant time/radius hardness ratio depends only on p , electron distribution index, and on the Lorentz invariant factor $\gamma_m^0 = \gamma_{\text{cc}}^2 \gamma_m^{-2}$ where:

$$\gamma_m^0 = \gamma_{\text{cc}}^2 \gamma_m^{-2} \quad (78)$$

is the minimum synchrotron characteristic frequency. Therefore by fitting observational data with (76) one can obtain

the index of the electron distribution and the time variation of Γ_m which is a very important quantity. Note that as $H R$ is time/radius dependent we need multiple energy bands and their hardness ratios to make a statistically meaningful fit. If we release the assumption of power-law distribution for electrons, we can use (62) to get insight into the distribution of electrons Lorentz factor and Γ_m , but they will be degenerate.

Once the energy and temporal behaviour of the integral term in (62) is found, the extraction of leading time dependent coefficient $F(r)$ (defined in (68)) from light curves is easy. Then if we use one of the models considered in this work or another model for the evolution of r , we can determine the time/radius variation of $\Gamma(r)$ the total Lorentz factor of the active region. Using (45) and (36) one can a priori estimate $M(r^0)$. However, the latter depends on the relative Lorentz factor $\Gamma(r^0)$. If we can roughly estimate the end of the collision from the form of the light curve – for instance if we assume that the end of the collision is when the continuous component begins an exponential decay – then:

$$f = \Gamma(r) \Big|_{r=r_f} \quad (79)$$

where r_f is the radius at which the coalescence of the shells finishes.

Γ_m^0 , $M(r^0)$, and $\Gamma_m(r^0)$ depend on the fundamental quantities such as magnetic field and thereby on the fraction of kinetic energy of the shell transferred to the electric and magnetic fields, the density of shells, and the initial distance of the collision from the central engine. But with only 3 quantities mentioned above we can not determine all these quantities and their time/radius variation. An important observable that can help to extract more information from data is the lag. If we neglect the term proportional to $G(r)$ and its derivatives, we can determine functions $P(r_0; \Gamma_m^0)$ and $Q(r_0; \Gamma_m^0)$ in (74) and (75) from the knowledge about $F(r)$ and the integral of $H(r)$ (defined in (69)) explained above. Thus in this way we can determine the lag between two energy bands. Comparison of the observed lags with the expectations from the model helps to estimate some of other quantities such as r_0 . However, as the analytical expression for the lags is very complex, only simulations and fits can permit to solve this inverse problem. Using a simpler version of the model presented here, this procedure has been applied to analyse the Swift data for GRB 060607a (Ziaepour et al. 2006b) and to explain some of its peculiar properties (Ziaepour et al. 2008a).

At the beginning of this section we mentioned that the most complete information about GRBs is in the spectrum at short time intervals when the flux does not change significantly. In fact in practice hardness ratios are calculated by adding together photons in a given energy band and time-rebinned event data to reduce the noise. When multiple simultaneous hardness ratios are available, they can be considered as a low resolution normalized spectrum in a short time interval. Because these quantities give the most direct insight into the physics of the collision, in the rest of this section we investigate in more details the spectral behaviour of the flux at constant time.

First we consider a power-law distribution for electrons. When $\Gamma_m^0 > \Gamma_m^0$ hypergeometric functions ${}_1F_2$ in (B4) and (B5) can be expanded as a polynomial with positive or zero

power of Γ_m^0 . This shows that at the lowest order in Γ_m^0 the spectrum $dP/d\Gamma_m^0 \propto (\Gamma_m^0)^{-2=3}$ and therefore $H R_{12} \propto (\Gamma_m^0)^{-2=3}$. The power of the coefficient in the second ${}_1F_2$ term is larger and therefore for determining the spectrum at zero order it can be neglected. But for the first order expansion of (B1) this term is significant and when it is added the spectrum becomes:

$$\frac{dP}{d\Gamma_m^0} \propto \left[(\Gamma_m^0)^{-2=3} + \frac{\frac{p}{4} + \frac{1}{6}}{2^{\frac{p}{4} + \frac{1}{6}}} (\Gamma_m^0)^{-2=3} \right] \quad \text{for } \frac{\Gamma_m^0}{\Gamma_m^0} < 1 \quad (80)$$

The amount of deviation from the dominant power-law only marginally depends on the index of the electron distribution function p . When $\Gamma_m^0 \gg \Gamma_m^0$ the higher power of Γ_m^0 becomes important and should be considered. However, as they are all positive, they make the spectrum harder. This result shows that although small hardening of the spectrum can be obtained in this regime, it is not possible to have a softer spectrum with an index smaller than $-2=3$ and closer to what has been observed in many bursts (Sakamoto et al. 2007, 2006). Note also that the addition of terms proportional to $G(r)$ can not make the spectrum softer because they have the same form of energy dependence as the dominant term s .

Next we consider the regime where $\Gamma_m^0 > \Gamma_m^0$. In this regime there is no analytical expression for ${}_1F_2$ functions. Therefore we use the asymptotic behaviour of Bessel functions, $K_0(x) \sim \sqrt{2\pi x} e^{-x}$, to estimate the integrals in (B1). Integration of the left hand side of (B4) leads to:

$$\begin{aligned} & \int_{\Gamma_m^0}^1 d\Gamma_m^0 \left(\frac{\Gamma_m^0}{\Gamma_m^0} \right)^{(p+1)} e^{-2\Gamma_m^0} \int_{\frac{\Gamma_m^0}{\Gamma_m^0}}^1 K_{5=3}(\Gamma_m^0) d\Gamma_m^0 \\ & \frac{1}{\Gamma_m^0} \left\{ \sqrt{2} \left(\frac{\Gamma_m^0}{\Gamma_m^0} \right)^{\frac{1}{2}} \left[\Gamma_m^0 (p+3); \left(\frac{\Gamma_m^0}{\Gamma_m^0} \right)^{\frac{1}{2}} \right] - \Gamma_m^0 (p+3); 1 \right\} + \\ & \left(\frac{\Gamma_m^0}{\Gamma_m^0} \right)^{\frac{p+2}{2}} \left[2^{\frac{1}{2}} \frac{\Gamma_m^0}{\Gamma_m^0} {}_1F_2 \left(\frac{p}{4} + \frac{1}{6}; \frac{1}{3}; \frac{p}{4} + \frac{7}{6}; \frac{1}{4} \right) + \right. \\ & \left. 2^{\frac{5}{3}} \left(\frac{\Gamma_m^0}{\Gamma_m^0} \right)^{\frac{2}{3}} {}_1F_2 \left(\frac{p}{4} + \frac{5}{6}; \frac{5}{3}; \frac{p}{4} + \frac{11}{6}; \frac{1}{4} \right) \right] \right\} \quad \text{for } \frac{\Gamma_m^0}{\Gamma_m^0} > 1 \quad (81) \end{aligned}$$

The constant coefficient in the last term is $1.354(2^{5=3} = (p+2=3) + 2^{1=3} = (p+10=3))$. Using an expansion in series of the incomplete function:

$$(a; x) = e^{-x} x^a \left[1 + \frac{1}{x} + \frac{1}{1+x} + \frac{1}{1+x} + \dots \right] \quad (82)$$

we see that in this regime at the lowest order the spectrum is a power-law with an index $-(1+p=2)$ which is much steeper (softer) than when $\Gamma_m^0 < \Gamma_m^0$. For energies between these two extreme regimes one expects an index $-(1+p=2) \dots -2=3$. They can be fitted by a power-law, but at high Γ_m^0 a power-law with an exponential cutoff gives a slightly better fit due to the presence of the exponential term in the expansion of the incomplete functions. Nonetheless if the distribution of electrons is truncated at high Lorentz factors or is a broken power-law in which the index becomes smaller at higher energies, this constraint will not be applicable. As $\Gamma_m^0 > \Gamma_m^0$, the second term in the sum and the last term in (81) are smaller than other terms considered above.

The two regimes explained above cover the maximum and soft wing of the index range observed by Swift

(Sakamoto et al. 2007) and BATSE but it can not explain very hard short bursts with indices larger than the zero order index $\alpha = 3$. Moreover, when the observed spectrum is extended to high energies, > 1 MeV, a power-law with an exponential cutoff at high energies is a better fit to GRBs spectrum. This type of spectra can be obtained if the distribution of the Lorentz factor of the accelerated electrons has an exponential cutoff at high energies. As we mentioned in Sec 2.2 the spectrum of the accelerated electrons in the simulations of ultra-relativistic shocks is more sophisticated than a simple power-law and is closer to a power-law with an exponential cutoff (Spitkovsky 2008), see (16). Assuming for simplicity an exact power-law with exponential cutoff for the Lorentz factor distribution of accelerated electrons like eq. (20), the dominant term of the spectrum (62) becomes proportional to:

$$\int_m^1 d\gamma \left(\frac{\gamma}{m} \right)^{(p+1)} e^{-\frac{\gamma}{p}} e^{-2 \int_{\frac{\gamma_0}{10}}^{\gamma} K_{5=3}(\gamma) d\gamma} \quad (83)$$

with the conditions mentioned in (20). When γ_{cut} the exponential term is close to 1 and the behaviour of the spectrum is indistinguishable from a simple power-law. But at high energies photons are emitted preferentially by faster electrons for which the exponential term is important and leads to an exponential cutoff in the spectrum of the synchrotron emission. To prove such a behaviour, we concentrate on the part of the spectrum for which $\gamma_0 = \frac{\gamma_0}{m} \ll 1$. In this case the integration of (83) leads to:

$$\begin{aligned} & \int_m^1 d\gamma \left(\frac{\gamma}{m} \right)^{(p+1)} e^{-\frac{\gamma}{p}} e^{-2 \int_{\frac{\gamma_0}{10}}^{\gamma} K_{5=3}(\gamma) d\gamma} \\ & \frac{\sqrt{2}}{m} \left[\int_1^{\left(\frac{\gamma_0}{m}\right)^{\frac{1}{2}}} dy y^{(p+3)} e^{-\frac{y}{p}} \left(\frac{1}{2} \left(\frac{\gamma_0}{m} y^2 \right) \right) + \right. \\ & \left. 2 \int_{\left(\frac{\gamma_0}{m}\right)^{\frac{1}{2}}}^1 dy y^{(p+3)} e^{-\frac{y}{p}} K_{2=3} \left(\frac{\gamma_0}{m} y^2 \right) \right] \quad (84) \end{aligned}$$

For $\gamma_0 = \frac{\gamma_0}{m} \ll 1$ the second integral on the right hand side of (84) is small and negligible. The first integral does not have analytical solution, but using asymptotic behaviour of incomplete γ function (82) one can conclude that its behaviour at high energies must be close to an exponential with negative exponent proportional to γ_0 .

In the beginning of this section we mentioned that most probably r is also somehow energy dependent, specially at very low and very high energies. In the latter case it must be very small, probably exponentially decreasing with energy. This can also contribute to the existence of an exponential cutoff at high energies. As for the low energy tail of the spectrum the fact that even the residual energy of cooled electrons can be enough to emit soft photons means that the spectrum in this regime should be much flatter. This is consistent with the roughly flat spectrum and shallow temporal decline in optical and longer wavelength emissions as observed in most GRBs (Roming et al. 2008; Oates et al. 2008).

In conclusion of this section, we showed that when a relativistic shock is modelled in details and realistic distributions for electrons are considered, the synchrotron emission alone can explain different aspects of the time averaged spectrum of GRBs as well as their spectrum in a short inter-

val in which the evolution can be ignored. Evidently, other processes such as inverse Compton (Kobayashi et al. 2007; Piran et al. 2008) and pair production (Amano et al. 2008) contribute to the total emission but most probably are not the dominant component at low / intermediate energy bands. Nonetheless their contribution should be more important at GeV and higher energies (Amano et al. 2008).

4 SUMMARY

We presented a formulation of the relativistic shocks and synchrotron emission that includes more details than the dominant term considered in the previous calculations. Although we consider spherical shells, most of our results are valid also for non-spherical collimated jets as long as the collimation angle due to the relativistic boost is smaller than collimation angle.

We showed that the lags between light curves at different energies exist in the dominant order and are not only due to the high latitude emissions which are negligible for ultra-relativistic ejecta. The main reason for such behaviour is the evolution of electric and magnetic fields as well as the evolution of the emitting region which can be in addition energy dependent. This fact is more evident in the simulations presented in Paper II. Despite the absence of high latitude terms in our simulations, the presence of lags between the light curves of different energy bands is evident. For the same reasons the change in the slope of the light curves – what is called breaks – are also energy dependent. This explains chromatic breaks of the GRBs detected by Swift.

The two phenomenological models we considered for the evolution of the active region are physically motivated, but do not have rigorous support from microphysics of the shock. Nonetheless, they can be easily replaced if future simulations of Fermi processes lead to a better estimation of the size of the region in which electric and magnetic fields are formed and particles are accelerated and dissipated. Presence of an external magnetic field in the environment of the candidates for central engine of GRBs is very plausible. The formulation present here does not include such a possibility, but an external magnetic field can be added to (23). The modification of the evolution equation of γ_0 and the flux is straightforward.

Many other details such as the effect of metallicity of the ejecta and surrounding material both on the low energy emission and absorption is not considered in this work. We have also neglected synchrotron self-absorption. It only affects the low energy bands, nonetheless in hard bursts even optical emission can be affected by self absorption. We leave the study of this issue, the effect of ionization on the emissions, and the thermalization of shocked material to future works.

APPENDIX A : ANALYTICAL APPROXIMATION OF $\gamma_0^{(1)}$

The integral in (37) can not be taken analytically. An analytical approximation is however useful for investigating the effect and importance of the radiation in the dynamics of the shell collision. Here we consider a few approximations

for various range of D and β that determine respectively the strength of the shock and the radiation.

If $\beta = 0$, the integral in §7) can be calculated analytically:

$$\int_0^{\frac{0}{(0)}(x^0)} dy \frac{1}{y^3(1-y^2)^3} = \left[A_1 \ln y + \frac{A_2}{y} + \frac{A_3}{2y^2} + B_1 \ln(y-1) + \frac{B_2}{y-1} + \frac{B_3}{2(y-1)^2} + C_1 \ln(y+1) + \frac{C_2}{y+1} + \frac{C_3}{2(y+1)^2} \right]_0^{\frac{0}{(0)}(x^0)} \quad (A1)$$

$$A_1 = 3; \quad A_2 = 0; \quad A_3 = 1; \quad B_1 = \frac{11}{8}; \quad B_2 = \frac{1}{2}; \quad B_3 = \frac{1}{8}; \quad C_1 = \frac{9}{16}; \quad C_2 = \frac{9}{16}; \quad C_3 = \frac{1}{8}; \quad (A2)$$

When $\beta = (3-D)$ is large, as the value of y in the integrand of (37) is always less than 1 we can formally expand the term $(1-y^2)^{-3} = 1 + 3y^2 + \dots$ and integrate term by term:

$$M_{(0)}(x^0) = \frac{r_0^0}{(3-D)} \left(\frac{0}{(0)} \right) [(3-D)]^{\frac{1}{3}} \left\{ \frac{1}{2+\frac{1}{3}} \left[\frac{0}{(0)} \right]^{\frac{2}{3}} {}_2F_1 \left[\frac{0}{(0)}; \frac{2}{3}; 1+\frac{0}{(0)} \right] + \frac{0}{(0)} \left[\frac{0}{(0)} \right]^{\frac{2}{3}} {}_2F_1 \left[\frac{0}{(0)}; \frac{2}{3}; 1+\frac{0}{(0)} \right] + \frac{(3-D)}{2+\frac{1}{3}} \left[\frac{0}{(0)} \right]^{\frac{2}{3}} {}_2F_1 \left[\frac{0}{(0)}; \frac{2}{3}; 1+\frac{0}{(0)} \right] + \frac{0}{(0)} \left[\frac{0}{(0)} \right]^{\frac{2}{3}} {}_2F_1 \left[\frac{0}{(0)}; \frac{2}{3}; 1+\frac{0}{(0)} \right] + \dots \right\} \quad (A3)$$

Here ${}_2F_1$ is the hypergeometric function and can be expanded as a polynomial of its last argument. When the latter is less than 1 and the power of the terms in the polynomial are positive, they converge rapidly to zero. When the last argument in ${}_2F_1$ is larger than one an analytical extension of this function with negative power in the polynomial expansion exists (Gradshteyn & Ryzhik 1980). Therefore, the dominant term is always $\frac{0}{(0)}$ in front of each ${}_2F_1$ term. For small β this approximation is not valid. In this case we ex-

pand $(1 + (\frac{1}{(3-D)} - \frac{1}{0})y)^{-3}$ and obtain:

$$M_{(0)}(x^0) = \frac{r_0^0}{(3-D)} \left(\frac{0}{(0)} \right) [(3-D)]^{\frac{1}{3}} \left\{ \frac{1}{2+\frac{1}{3}} \left[\frac{0}{(0)} \right]^{\frac{2}{3}} {}_2F_1 \left[\frac{0}{(0)}; \frac{2}{3}; 1+\frac{0}{(0)} \right] + \frac{0}{(0)} \left[\frac{0}{(0)} \right]^{\frac{2}{3}} {}_2F_1 \left[\frac{0}{(0)}; \frac{2}{3}; 1+\frac{0}{(0)} \right] + \frac{0}{(0)} \left[\frac{0}{(0)} \right]^{\frac{2}{3}} {}_2F_1 \left[\frac{0}{(0)}; \frac{2}{3}; 1+\frac{0}{(0)} \right] + \dots \right\} \quad (A4)$$

In the same way we find the following expression for $M_{(0)}(x^0)$ for the quasi-steady model and large $\beta = (3-D)$:

$$M_{(0)}(x^0) = \frac{r_1}{3} [(3-D)]^{\frac{1}{3}} \left\{ \left\{ \frac{1}{3} \left[\frac{0}{(0)} \right]^{\frac{2}{3}} {}_2F_1 \left[\frac{0}{(0)}; \frac{2}{3}; 1+\frac{0}{(0)} \right] + \frac{0}{(0)} \left[\frac{0}{(0)} \right]^{\frac{2}{3}} {}_2F_1 \left[\frac{0}{(0)}; \frac{2}{3}; 1+\frac{0}{(0)} \right] + \frac{0}{(0)} \left[\frac{0}{(0)} \right]^{\frac{2}{3}} {}_2F_1 \left[\frac{0}{(0)}; \frac{2}{3}; 1+\frac{0}{(0)} \right] + \dots \right\} + \frac{1}{3} \left[\frac{0}{(0)} \right]^{\frac{2}{3}} {}_2F_1 \left[\frac{0}{(0)}; \frac{2}{3}; 1+\frac{0}{(0)} \right] + \frac{0}{(0)} \left[\frac{0}{(0)} \right]^{\frac{2}{3}} {}_2F_1 \left[\frac{0}{(0)}; \frac{2}{3}; 1+\frac{0}{(0)} \right] + \frac{0}{(0)} \left[\frac{0}{(0)} \right]^{\frac{2}{3}} {}_2F_1 \left[\frac{0}{(0)}; \frac{2}{3}; 1+\frac{0}{(0)} \right] + \dots \right\} \quad (A5)$$

For the case of a small $\beta = (3-D)$ one can use (A4) and make an expression analogue to (A5), thus we do not repeat the details here. We note that when $\beta = 0$ and $\beta \rightarrow 1$, i.e. for a constant r^0 , (A3) and (A5) are equal as expected. When $\beta \rightarrow 0$, the formation of the active region is very slow. In this case the energy loss by radiation becomes negligible and decreases only due to the increasing accumulated mass. Note also that $M_{(0)}(x_0) = 0$ as expected. If the active region varies according to (29), the expression for $M_{(0)}(x^0)$ includes only the term $\beta + \dots$ in (A5) with a positive sign in front.

Although equations (A3), (A5), and (A4) seem quite sophisticated, due to the polynomial representation of ${}_2F_1$, only the few dominant terms are of real interest to us. In most cases we are only interested in the dominant power-law component. However, having expressions beyond the dominant power permits to go much further and calculate quantities such as lags that in a simple power-law approximation can not be determined.

When the kinetic energy of the fast shell does not change significantly $\frac{0}{(0)}(x^0) = \frac{0}{(0)}$ and $M_{(0)}(x) \neq 0$. This case happens when the radiation has a negligible effect on the kinematic of the shock. Assuming a strong shock i.e.

$\frac{\omega_0}{\omega_{ce}} < 3D$, we can use the definition of ${}_2F_1$ to investigate the behaviour of $M_{(0)}(r)$ at lowest order. For the dynamically driven active region with large β and a relatively soft shock, when we expand ${}_2F_1$ term in (A 3) up to first order, $M_{(0)}(r)$ becomes:

$$M_{(0)}(r^0) = \frac{r_0^0}{(3)} \left(\frac{0}{0} \right) (3) D^{\frac{1}{3}} \frac{0}{0} \frac{2}{3} \frac{0}{0} \left\{ \frac{1}{3} \left(1 - \frac{0}{(3)} D \right) \left[\frac{1}{1 + \frac{0}{3}} \left(1 - \frac{0}{(0)} \frac{r^0}{0} \right)^{1 + \frac{0}{3}} \right] + \frac{(3) \frac{0}{2} \frac{0}{0}^2}{1 + \frac{0}{3}} \left(1 - \frac{0}{(0)} \frac{r^0}{0} \right)^{1 + \frac{0}{3}} \right] + \dots \} \quad (A 6)$$

Similarly, for small β we use (A 4) and obtain:

$$M_{(0)}(r^0) = \frac{r_0^0}{(3)} \left(\frac{0}{0} \right) (3) D^{\frac{1}{3}} \frac{0}{0} \frac{2}{3} \frac{0}{0} \left\{ \left[1 + \frac{(3) \frac{0}{2} \frac{0}{0}^2}{1 + \frac{0}{3}} + \frac{1}{3} \left(1 - \frac{0}{(3)} D \right) \left(1 + \frac{(3) \frac{0}{2} \frac{0}{0}^2}{1 + \frac{0}{3}} \right) \right] \left(\frac{0}{(0)} \frac{r^0}{0} \right)^{2 + \frac{0}{3}} \left[1 + \frac{(3) \frac{0}{2} \frac{0}{(0)}^2 \frac{r^0}{0}}{1 + \frac{0}{3}} + \frac{0}{(3)} \frac{r^0}{0} \left(1 - \frac{0}{(3)} D \right) \left(1 + \frac{(3) \frac{0}{2} \frac{0}{(0)}^2 \frac{r^0}{0}}{1 + \frac{0}{3}} \right) \right] \right\} \quad (A 7)$$

For a quasi-static active region and the same shock conditions as in (A 5) the first order $M_{(0)}(r)$ is:

$$M_{(0)}(r^0) = \frac{r_1^0}{(3)} \left(\frac{0}{0} \right) (3) D^{\frac{1}{3}} \frac{0}{0} \frac{2}{3} \frac{0}{0} \left\{ \frac{1}{3} \left[\frac{1}{1 - \frac{0}{(0)} \frac{r^0}{0}^2} - \frac{0}{(0)} \frac{r^0}{0}^{\frac{0}{3} + 1} \right] + \frac{3}{\frac{0}{3} + 1} \left(\frac{0}{(0)} \frac{r^0}{0}^{\frac{0}{3} + 1} \right) \right\} + \dots$$

APPENDIX B: SPECTRUM AND LAGS FOR POWER-LAW AND EXPONENTIAL ELECTRON DISTRIBUTIONS

Using (13) to (15), after integration over e we obtain the following expression for the spectrum:

$$\frac{dP}{d\omega} = \frac{P_0 e^2}{3} r^2 r \frac{N_e}{\omega^4(r) (1 - \frac{0}{(r)})^{\frac{0}{3}}} \left\{ 2 \int_0^1 d\left(\frac{e}{m} \right)^{(p+1)} e^2 \int_{\frac{1}{10}}^1 K_{5=3}(\omega) d\omega + G(r) \left[\frac{11}{12 m} \left[\frac{2^{\frac{2}{3}} \left(\frac{1}{10} \right)^{\frac{1}{3}}}{\frac{p}{4} + \frac{1}{3}} \right] {}_1F_2 \left(\frac{p}{4} + \frac{1}{3}; \frac{2}{3}; \frac{p}{4} + \frac{4}{3}; \left(\frac{1}{2! m} \right)^2 \right) + \frac{2^{\frac{4}{3}} \left(\frac{1}{10} \right)^{\frac{1}{3}}}{\frac{p}{4} + \frac{2}{3}} \left(\frac{1}{3} \right) {}_1F_2 \left(\frac{p}{4} + \frac{2}{3}; \frac{4}{3}; \frac{p}{4} + \frac{5}{3}; \left(\frac{1}{2! m} \right)^2 \right) \right] \right. \\ \left. \frac{21}{8 m} \left[\frac{2^{\frac{1}{3}} \left(\frac{1}{10} \right)^{\frac{2}{3}}}{\frac{p}{4} + \frac{2}{3}} \left(\frac{2}{3} \right) {}_1F_2 \left(\frac{p}{4} + \frac{2}{3}; \frac{1}{3}; \frac{p}{4} + \frac{5}{3}; \left(\frac{1}{2! m} \right)^2 \right) + \frac{2^{\frac{5}{3}} \left(\frac{1}{10} \right)^{\frac{2}{3}}}{\frac{p}{4} + \frac{4}{3}} \left(\frac{2}{3} \right) {}_1F_2 \left(\frac{p}{4} + \frac{4}{3}; \frac{5}{3}; \frac{p}{4} + \frac{7}{3}; \left(\frac{1}{2! m} \right)^2 \right) \right] + \frac{7}{4} \frac{2}{m} \left(\frac{1}{10} \right) \int_0^1 d\left(\frac{e}{m} \right)^{(p+1)} e^4 \int_{\frac{1}{10}}^1 K_{5=3}(\omega) d\omega \right\} \quad (B 1)$$

where $\omega_{cc}^0 = \omega_{cc}^0 \frac{2}{m}$ is the minimum characteristic frequency of electrons. The double integrals in the first and last term of (B 1) do not have a simple analytical expression. An approximation can be obtained using an integral form of K Bessel function:

$$K_1(\omega) = \int_0^1 dx e^{-\omega x} \frac{1}{\omega x} \quad (B 2)$$

$$\int_0^1 K_1(\omega) d\omega = \int_0^1 dx \frac{1}{\omega x} e^{-\omega x} = 2K_1(\omega) \quad (B 3)$$

The last integral is small and can be neglected. Therefore:

$$\int_m^1 d e \left(\frac{e}{m} \right)^{(p+1)} e^{-2} \int_{\frac{1}{10}}^1 K_{5=3}(\cdot) d$$

$$\frac{1}{2} \left[\frac{2^{\frac{1}{3}} \left(\frac{1}{10} \right)^{\frac{2}{3}}}{\frac{p}{4} + \frac{1}{6}} {}_1F_2 \left(\frac{p}{4} + \frac{1}{6}; \frac{1}{3}; \frac{p}{4} + \frac{7}{6}; \right. \right.$$

$$\left. \left(\frac{1}{2!} \right)^2 \right) + \frac{2^{\frac{5}{3}} \left(\frac{1}{10} \right)^{\frac{2}{3}}}{\frac{p}{4} + \frac{5}{6}} {}_1F_2 \left(\frac{p}{4} + \frac{5}{6}; \frac{5}{3}; \right.$$

$$\left. \frac{p}{4} + \frac{11}{6}; \left(\frac{1}{2!} \right)^2 \right) \right] \quad (B4)$$

$$\int_m^1 d e \left(\frac{e}{m} \right)^{(p+1)} e^{-4} \int_{\frac{1}{10}}^1 K_{5=3}(\cdot) d$$

$$\frac{1}{2} \left[\frac{2^{\frac{1}{3}} \left(\frac{1}{10} \right)^{\frac{2}{3}}}{\frac{p}{4} + \frac{2}{3}} {}_1F_2 \left(\frac{p}{4} + \frac{2}{3}; \frac{1}{3}; \frac{p}{4} + \right. \right.$$

$$\left. \frac{5}{3}; \left(\frac{1}{2!} \right)^2 \right) + \frac{2^{\frac{5}{3}} \left(\frac{1}{10} \right)^{\frac{2}{3}}}{\frac{p}{4} + \frac{4}{3}} {}_1F_2 \left(\frac{p}{4} + \frac{4}{3}; \frac{5}{3}; \right.$$

$$\left. \frac{p}{4} + \frac{7}{3}; \left(\frac{1}{2!} \right)^2 \right) \right] \quad (B5)$$

If the electron distribution is exponential i.e. $n_e^0(e) = N_e \exp(-e)$, term with ${}_1F_2$ must be replaced by terms proportional to Meijer's G-functions. These functions do not have simple analytical presentations. Therefore only asymptotic behaviour of power spectrum is described in Sec. 2.4.

In the same way we can determine an analytical expression for lags when accelerated electrons have a power-law distribution using (65) to (75) and (B1) to (B5). In fact, it is easy to see that the functions $P(r_0; \frac{1}{10})$ and $Q(r_0; \frac{1}{10})$ are both functionals of H which contains e dependent terms similar to the spectrum $dP = d!$. The function H includes Bessel and hypergeometric functions and their derivatives. Therefore we can use (B1) to (B5) to determine them. As the derivatives of hypergeometric functions ${}_1F_2(\cdot; \cdot; z)$ are also hypergeometric, lags can be expressed as a sum of ${}_1F_2$ functions. The calculation is straightforward but long and laborious and we do not present details here because their complexity does not permit to investigate their properties and numerical calculation is needed.

ACKNOWLEDGMENTS

I would like to thank Keith Mason for encouraging me to work on GRB science. The ideas presented in this work couldn't be developed without long discussions with the past and present members of the Swift science team at MSSSL: A. Blustin, A. Breveveld, M. De Pasquale, P. Kuin, S. Oates, S. Rosen, M. Page, P. Schady, M. Still, and S. Zane, as well as the other members of the Swift team in particular: S. Barthelmy, Ph. Evens, E.E. Fenimore, N. Gehrels, P. Meszaros, J. Osborne, and K. Page. I thank all of them.

REFERENCES

- Anile, A.M., "Relativistic fluids and magneto-fluids", Cambridge University Press (1989).
- Asano, K., Inoue, S., & Meszaros, P., (2008), arXiv:0807.0951.
- Barthelmy, S.D., Cummings J.R., Fenimore E., Gehrels N., Hullinger D., Krimm H.; Markwardt C., et al, Space Sci. Rev. 120, (2005) 143, astro-ph/0507410.
- Bednarz, J. & Ostrowski, M., MNRAS 283, (1996) 447, astro-ph/9608078.
- Blandford, R.D. & McKee, C.F., Phys. of Fluids 19, (1977) 1130.
- Blasi, P. & Vietri, M., ApJ. 626, (2005) 877, astro-ph/0503220.
- Bradley Cenko, S., submitted (2008), arXiv:0802.0874.
- Burrows, D.N., Hill J.E., Nousek J.A., Kennea J.A., Wells A., Osborne J.P., Abbey A.F., Beardmore, A., et al, Space Sci. Rev. 120, (2005) 165, astro-ph/0508071.
- Cenko, S.B., Kasliwal, M., Harrison, F.A., Palshin, V., Frail, D.A., et al, ApJ. 652, (2006) 490, astro-ph/0608183.
- Chevalier, R.A. & Li, Z.-Y., ApJ. 536, (2000) 195, astro-ph/9908272.
- Corsi, A. & Piro, L., A & A. 458, (2006) 741, astro-ph/0604158.
- Covino, S., Malesani, D., Tagliaferri, G., Vergani, S.D., Chincarini, G., et al, Nuovo Cimento B 121, (2006) 1171, astro-ph/0612643.
- Dai, Z.G., Zhang, B., & Liang, E.W., (2006), astro-ph/0604510.
- Dai Z.G. & Lu, T., A & A. 333, (1998) L87, astro-ph/9810402.
- Daigne, F. & Mochkovitch, R., MNRAS 296, (1998) 275, astro-ph/9801245.
- Daigne, F. & Mochkovitch, R., MNRAS 342, (2003) 587, astro-ph/0303287.
- Dempsey, P. & Dwyer, P., MNRAS 378, (2007) 625, arXiv:0704.0168.
- De Pasquale, M., Evans, Ph.A., Oates, S., Page, M., Zane, S., et al (2008), arXiv:0809.4688.
- Dieckmann, M.E., Sironi, N.J., Parviainen, M., Shukla, P.K., & Dendy, R.O., Plasma Phys. Control Fusion 48, (2006) 489, astro-ph/0602337.
- Eldridge, J.J., Genet, F., Daigne, F., & Mochkovitch, R., MNRAS 367, (2006) 186, astro-ph/0509749.
- Fan, Y.Z. & Wei, D.M., MNRAS 364, (2005) 42, astro-ph/0506155.
- Fenimore, E.E., in't Zand, J.J.M., Norris, J.P., Bonnell, J.T., & Nemiro, R.J., ApJ. 101, (1995) 448L, astro-ph/9504075.
- Fenimore, E.E., Madras, C.D., & Nayakshin, S., ApJ. 473, (1996) 998, astro-ph/9607163.
- Fenimore, E.E. & Ramirez-Ruiz, E., (1999), astro-ph/9909299.
- Foley, S., McGlynn, S., Hanlon, L., McBrean, S., & McBrean, B., (2008), arXiv:0803.1821.
- Fryer, C.L., Rockefeller, G., & Young, P.A., ApJ. 647, (2006) 1269, astro-ph/0604432.
- Gal-Yam, A., Nakar, E., Ofek, E.O., Cenko, S.B., Kulkarni, S.R., et al, ApJ. 686, (2008) 408, astro-ph/0509891.
- Gehrels, N., Chincarini, G., Giommi, P., Mason, K.O.,

- Nousek, J.A., Wells, A.A., White, N.E., Barthelmy, S.D., et al., *ApJ*. 611, (2004) 1005, astro-ph/0405233.
- Gehrels, N., et al. *Nature* 444, (2006) 1044, astro-ph/0610635
- GradshTEyn, I.S. & Ryzhik, I.M., "Table of integrals, series, and products", Academic Press, INC. (1980).
- Guidorzi, C., Baumgartner, W.H., Beardmore, A.P., Cummings, J., Gehrels, N., et al., *GCN Circ.* 8421, *GCN Rep.* 176.1, (2008).
- Holland, S.T., Barthelmy, S.D., Burrows, D.N., Gehrels, N., S. Hunsberger, S., et al., *GCN Circ.* 4570, (2006).
- Huang, Y.F., Gou, L.J., Dai, Z.G., Lu, T., *ApJ*. 543, (2000) 90.
- Jackson, J.D., "Classical electrodynamics", John Wiley & Sons INC. (2001).
- Keshet, U., Katz, B., Spitkovsky, A., & Waxman, E., (2008), arXiv:0802.3217.
- Kobayashi, S., *ApJ*. 545, (2000) 807, astro-ph/0009319.
- Kobayashi, Sh., Zhang, B., Meszaros, P., & Burrows, D.N., *ApJ*. 655, (2007) 391, astro-ph/0506157.
- Kouveliotou, C., Meegan, C.A., Fishman, G.J., Bhat, N.P., Briggs, M.S., Koshut, T.M., Paciesas, W.S., & Pendleton, G.N., *ApJ*. 413, (1993) L101.
- Krimm, H.A., Barthelmy, S.D., Chester, M.M., Cusumano, G., Evans, P.A., et al., *GCN Circ.* 6005, *GCN Rep.* 263, (2007).
- Kumar, P., McMahon, E., Barthelmy, S.D., Burrows, D., Gehrels, N., Goad, M., Nousek, J., & Tagliaferri, G., *MNRAS* 367, (2006) L52, astro-ph/0602060.
- Lazzati, D., Morsony, B.J., & Begelman, M.C., *Nuovo Cimento B* 121, (2006) 1177, astro-ph/0612320.
- Lazzati, D., Morsony, B.J., & Begelman, M.C., *PhilTransRoy.Soc.Lond. A* 365, (2007) 1141, astro-ph/0611192.
- Lu, R.J., Qin, Y.P., Zhang, Z.B., & Yi, T.F., *MNRAS* 367, (2006) 275, astro-ph/0509287.
- Manganò, V., Holland, S.T., Malesani, D., Troja, E., Chincarini, G., et al. *A & A*. 470, (2007) 105, arXiv:0704.2235.
- Manganò, V., Cummings, J., Cusumano, G., Gehrels, N., La Parola, V., et al., *GCN Circ.* 7847, *GCN Rep.* 147.1, (2008).
- Mao, J., Baumgartner, W.H., D.N. Burrows, D.N., Chester, M.M., Gehrels, N., et al., *GCN Circ.* 7665, *GCN Rep.* 138.1, (2008).
- Meszaros, P., *AIPC* 906, (2007) 40, astro-ph/0601661.
- Misra, K., Bhattacharya, D., Sahu, D.K., Sagar, R., Anupama, G.C., Castro-Tirado, A.J., Guziy, S.S., Bhatt, B.C., A & A. 464, (2007) 903, astro-ph/0701413.
- Morette, A., Barthelmy, S.D., Cummings, J.R., Guidorzi, C., Markwardt, C.B., et al. *GCN Circ.* 5442, (2006).
- Nakar, E. & Granot, J., *MNRAS* 380, (2007) 1744, astro-ph/0606011.
- Nakar, E. & Piran, T., *MNRAS* 353, (2004a) 647, astro-ph/0403461.
- Norris, J.P., Marani, G.F., & Bonnell, J.T., *ApJ*. 534, (2000) 248, astro-ph/9903233.
- Oates, S.R., Page, M.J., Schady, P., de Pasquale, M., Koch, T.S., et al., to be published in *MNRAS* (2009), arXiv:0901.3597.
- Pagani, C., Barthelmy, S.D., Cummings, J., Gehrels, N., Grupe, D., et al., *GCN Circ.* 4867, (2006).
- Page, M., Burrows, D., Beardmore, A., Palmer, D., Kennea, J., et al., *GCN Circ.* 3830, (2005).
- Panaitescu, A., Meszaros, P., Burrows, Nousek, J., Gehrels, N., O'Brien, P., & Willingale, R., *MNRAS* 369, (2006) 2059, astro-ph/0604105.
- Panaitescu, A. & Vestrand, W.T., *MNRAS* 387, (2008) 497, arXiv:0803.1872.
- Panaitescu, A. & Meszaros, P., *ApJ*. 493, (1998) L31, astro-ph/9709284.
- Panaitescu, A., *MNRAS* 362, (2005) 921, astro-ph/0506577.
- Pe'er, A., & Zhang, B., *ApJ*. 653, (2006) 454, astro-ph/0605641.
- Petrovic, J., Langer, N., Yoon, S.-Ch., & Heger, A., *A & A*. 435, (2005) 1013, astro-ph/0504175.
- Piran, T., Shemi, A., & Narayan, R., *MNRAS* 263, (1993) 861, astro-ph/9301004.
- Piran, T., Sari, R., & Zou, Y.-Ch., (2008), arXiv:0807.3954.
- Qin, Y.P., A & A. 396, (2002) 705.
- Qin, Y.P., Zhang, Z.B., Zhang, F.W., & Cui, X.H., *ApJ*. 617, (2004) 439, astro-ph/0401180.
- Ramirez-Ruiz, E. & Granot, J., *New Astron.* 12, (2007) 630, astro-ph/0608379.
- Racusin, J.L., Barthelmy, S.D., Burrows, D., Chester, M.M., Gehrels, N., et al. *GCN Circ.* 6620, *GCN Rep.* 70.1, (2007).
- Racusin, J.L., Gehrels, N., Holland, S.T., Kennea, J., Markwardt, C.B., et al. *GCN Circ.* 7427, *GCN Rep.* 134.1, (2008a).
- Racusin, J.L., Karpov, S.V., Sokolowski, M., Granot, J., Wu, X.F., et al., *Nature* 455, (2008b) 183, arXiv:0805.1557.
- Rees, M.J., *MNRAS* 135, (1967) 345.
- Rees, M.J. & Meszaros, P., *ApJ*. 430, (1994) L93, astro-ph/9404038.
- Rees, M.J. & Meszaros, P., *ApJLett.* 496, (1998) L1, astro-ph/9712252.
- Rees, M.J., Meszaros, P., & Wijers, R.A.M.J., *ApJ*. 499, (1998) 301, astro-ph/9709273.
- Rees, M.J. & Meszaros, P., *ApJ*. 545, (2000) L73, astro-ph/0010258.
- Reville, B., Kirk, J.G., & Du, P., *Plasma PhysControlFusion* 48, (2006) 1741, astro-ph/0608462.
- Rhoads, J.E., *ApJ*. 525, (1999) 737, astro-ph/9903399.
- Rieger, F.M., Bosch-Ramon, V., & Du, P., *Astrophys.SpaceSci.* 309, (2007) 119, astro-ph/0610141.
- Romano, P., Moretti, A., Banat, P.L., Burrows, D., Campana, S., et al., *A & A*. 450, (2006) 59, astro-ph/0601173.
- Romano, P., Campana, S., Chincarini, G., Cummings, J., Cusumano, G., et al., *Nuovo Cimento B* 121, (2008) 1067, astro-ph/0612494.
- Roming, P.W.A., Kennedy, T.E., Mason, K.O., Nousek, J.A., Ahl, L., Bingham, R.E., Brooks, P.S., Carter, M.J., et al., *Space Sci. Rev.* 120, (2005) 95, astro-ph/0507413.
- Roming, P.W.A., Vanden Berk, D., Palshin, V., Pagani, C., Norris, J., et al., *ApJ*. 651, (2006) 985, astro-ph/0605005.
- Roming, P.W.A., Koch, T.S., Oates, S., Porter, B.L., Vanden Berk, D., et al., (2008), arXiv:0809.4193.
- Rybicki, G.B. & Lightman, A.P., "Radiative Processes in Astrophysics", Wiley-VCH (2004).
- Sadun, A.C. & Sadun, L.A., *Astrophys.SpaceSci.* 185,

- (1991) 21.
- Sakamoto, T., Barbier, L., Barthelmy, S.D., Cummings, J., Fenimore, E., et al., proceedings of "Gamma Ray Bursts in the Swift Era", eds. S. Holt, N. Gehrels & J. Nousek, (2006), astro-ph/0605717.
- Sakamoto, T., Barthelmy, S.D., Barbier, L., Cummings, J., Fenimore, E., et al., (2007), arXiv:0707.4626.
- Sari, R. & Piran, T., ApJ. 455, (1995) L143, astro-ph/9508081.
- Sari, R., Narayan, R., & Piran, T., ApJ. 473, (1996) 204, astro-ph/9605005.
- Sari, R., Piran, T., & Narayan, R., ApJ. 497, (1998) 17, astro-ph/9712005.
- Sari, R., Piran, T., & Halpern, J.P., ApJLett. 636, (1999) L73, astro-ph/9903339.
- Sari, R. & Meszaros, P., ApJ. 535, (2000) L33, astro-ph/0003406.
- Sato, G., Campana, S., Evans, P.A., Guidorzi, C., Markwardt, C.B., et al., GCN Circ. 6352, GCN Rep. 50.1, (2007a).
- Sato, G., Yamazaki, R., Ioka, K., Sakamoto, T., Nakazawa, K., et al., ApJ. 657, (2007b) 359, astro-ph/0611148.
- Schady, P., Burrows, D., Cummings, J., Gehrels, N., Guidorzi, C., et al., GCN Circ. 5699, GCN Rep. 6.1, (2006a).
- Schady, P., Cummings, J., Guidorzi, C., Pagani, C., Palmer, D., et al., GCN Circ. 5707, GCN Rep. 7.1, (2006b).
- Schady, P., De Pasquale, M., Cummings, J., Page, M.J., Pandey, S.B., et al., MNRAS 380, (2007) 1041, astro-ph/0611089.
- Schwinger, J., Phys. Rev. 75, (1949) 1912.
- Silva, L.O., Fonseca, R.A., Tonge, J.W., Mori, W.B., & Dawson, J.M., Phys. Plasma 9, (2002) 2458.
- Soderberg, A.M., Kulkarni, S.R., Nakar, E., Berger, E., Fox, D.B., et al., Nature 442, (2006) 1014, astro-ph/0604389.
- Spitkovsky, A., ApJ. 682, (2008) 5, arXiv:0802.3216.
- Stamatikos, M., Barthelmy, S.D., Chester, M.M., Cusumano, G., Landsman, W.B., et al., GCN Circ. 5999, GCN Rep. 25.1, (2007).
- Stern, B.E. & Poutanen, J., MNRAS 352, (2004) L35, astro-ph/0405488.
- Takami, K., Yamazaki, R., Sakamoto, T., & Sato, G., ApJ. 663, (2007) 1118, arXiv:0704.1055.
- Troja, E., Cusumano, G., O'Brien, P., Zhang, B., Sbarufatti, B., et al., ApJ. 665, (2007) 599, astro-ph/0702220.
- Umeda, H., Tomonaga, N., Mada, K., & Nomoto, K., ApJ. 633, (2005) L17, astro-ph/0509750.
- van Eerten, H.J. & Wijers, R.A.M.J., To appear in proceedings of "6th Huntsville symposium " conference, 20-23 October 2008, (2009), arXiv:0902.0233.
- Vietri, M., ApJ. 591, (2003) 954, astro-ph/0212352.
- Vigeli, M., Melatos, A., Chatterjee, S., Gaensler, B.M., & Ghavamian, P., MNRAS 374, (2007) 793, astro-ph/0610454.
- Virtanen, J.J.P. & Vainio, R., ApJ. 621, (2005a) 313, astro-ph/0411184.
- Virtanen, J.J.P. & Vainio, R., A & A. 439, (2005b) 439, astro-ph/0505598.
- Wang, X.Y., Dai, Z.G., & Lu, T., ApJ. 556, (2001) 1010, astro-ph/0104128.
- Wang, X.-Y. & Meszaros, P., ApJ. 670, (2007) 1247, astro-ph/0702441.
- Watson, D., Hjorth, J., Fynbo J.P.U., Jakobsson P., Foley S., Sollerman J., Wijers R.A.M.J., ApJ. 660, (2007) L101, astro-ph/0702537.
- West, K.C., ApJ. 130, (1959) 241.
- Wiersema, J. & Achterberg, A., A & A. 428, (2004) 365, astro-ph/0408550.
- Wijers, R.A.M.J. & Galama, T.J., ApJ. 523, (1999) 177.
- Xu, L., Wu, X.F., & Dai, Z.G., ApJ. 634, (2005) 1155, astro-ph/0508324.
- Yang, T.Y.B., Amos, J., & Langdon, A.B., Phys. Plasma 1, (1994) 3059.
- Zhang, B. & Meszaros, P., ApJ. 566, (2002) 712, astro-ph/0108402.
- Zhang, B. & Kobayashi, Sh., ApJ. 628, (2005) 315, astro-ph/0404140.
- Zhang, B., Fan, Y.Z., Dyks, J., Kobayashi, Sh., Meszaros, P., et al., ApJ. 642, (2006) 354, astro-ph/0508321.
- Zhang, B., Zhang, B.B., Liang, E.W., Gehrels, N., Burrows, D.N., Meszaros, P., ApJ. 655, (2007a) L25, astro-ph/0612238.
- Zhang, B.B., Liang, E.W., & Zhang, B., ApJ. 666, (2007b) 1002, astro-ph/0612246.
- Ziaee, P., Blustin, A., Burrows, D., Cummings, J., et al., GCN Circ. 4429, (2006a).
- Ziaee, P., Barthelmy, S.D., Gehrels, N., Goad, M.R., Kennea, J., et al., GCN Circ. 5233, (2006b).
- Ziaee, P., Barthelmy, S.D., Beardmore, A.P., Burrows, D., De Pasquale, M., et al., GCN Circ. 6654, GCN Rep. 74.2, (2007a).
- Ziaee, P., Barthelmy, S.D., Beardmore, A.P., Burrows, D., Evans, P.A., et al., GCN Circ. 6640, GCN Rep. 73.2, (2007b).
- Ziaee, P., Holland, S.T., Boyd, P.T., Page, K., Oates, S., et al., MNRAS 385, (2008a) 453, arXiv:0712.3269.
- Ziaee, P., Barthelmy, S.D., Baumgartner, W.H., Beardmore, A.P., Burrows, D., et al., GCN Circ. 7639, GCN Rep. 130.1, (2008b).